ISTANBUL TECHNICAL UNIVERSITY ★ INSTITUTE OF SCIENCE AND TECHNOLOGY

MESH GENERATION FOR THE SHIP-WAVE PROBLEM

M.Sc.THESIS

Şafak Nur ERTÜRK, B.Sc.

Date of Submission : 12 June 1995
Date of Approval : 28 June 1995
Examination Commitee
Supervisor : Assistant Prof. Dr. Muhittin SÖYLEMEZ
Member : Prof Dr. L. Macit SÜKAN
Member : Associate Prof. Dr. Ömer GÖREN

JUNE, 1995

PREFACE

Grateful acknowlegments are due to several people.

Firstly I would like to thank to Dr. Muhittin SÖYLEMEZ for all the help and support he had given to me in this study. Also I am indebted to Dr. Ömer GÖREN for his constructive discussions and help in terms of valuable knowledge and material.

I would like to thank to Dr. Kadir SARIÖZ who has made many suggestions for the development of the programmes and to Mr. A.Murat GÖKMEN without whom transfering programmes and data between a PC and an Apollo HP would have been impossible. Special thanks are for my friend, Mr. Özgür GÜRGEY, who has put an effort into correction of errors and also made many suggestions for improvements.

I would like to express my sincere thanks to my parents who gave endless support and encouragement throughout this study.

Any errors that may appear are, of course, the responsibility of the author. She will very much appreciate having these brought to her attention.

June, 1995 Şafak Nur ERTÜRK

TABLE OF CONTENTS

NOMENCLATURE

$\partial/\partial n$: differentiation in the direction of outward normal to the surface S at point p.

Φ : scalar potential function.

Φ_{ij} : potential that is induced at the control point of the ith element by a unit source density on the jth element.

ρ : constant fluid density.

$\sigma(q)$: local intensity of source distribution.

φ : potential function.

φ_i : perturbation potential due to the body surface.

A_{ij} : the normal velocity induced at the control point of the ith element by a unit source density of the jth element.

B_i : constant coefficients.

C_p : pressure coefficient.

E : Young's modulus.

F : known function of position and time on S.

$[F]$: blending function matrix.

$[G]$: matrix of geometric conditions.

I : moment of inertia.

i,j,k : unit vectors along the axes of the reference co-ordinate system in

which the body surface is put.

$M(x)$: bending moment.

$\mathbf{n}$: unit outward normal vector at a point of S.

$\mathbf{n}_i$: unit normal vector to the ith element.

p : fluid pressure.

p_∞ : pressure at infinity.

$P(t)$: position vector of any point on the cubic spline segment.

$P'(t)$: tangent vectors at the ends of the spline segment.

$r(P,q)$: distance between P and q.

$R(x)$: radius of curvature of the beam.

q : a general point on the surface S.

S : boundary of region R'.

t_1, t_2 : parameter values at the beginning and end of the segment.

$\mathbf{v}$: disturbance velocity field due to the boundaries.

$\mathbf{V}$: fluid velocity.

$\mathbf{V}_i$: potential velocity including the effects of the onset flow.

$\mathbf{V}_{ij}$: velocity that is induced at the control point of the ith element by a unit source density on the jth element.

$\mathbf{V}_\infty$: velocity of the onset flow.

x,y,z : co-ordinates of point P.

X_{ij},Y_{ij},Z_{ij} :components of $\vec{V}_{ij}$.

x_q,y_q,z_q : co-ordinates of point q.

y : deflection of the beam.

LIST OF FIGURES

* free surface panels are prepared manually by using real streamlines

SUMMARY

MESH GENERATION FOR THE SHIP WAVE PROBLEM

The improvement of a ship hull form is an important development in the field of ship hydrodynamics. The ship hull form affects the wave-making characteristics of the ship. These effects have been explored by using different theories. One of these theories is the thin-ship theory. In the method of the thin-ship theory, equivalent sources representing ship form are distributed on the centerplane of the ship on the assumption that the breadth of the ship is very small in comparison with its length. However most of the ships built are not so thin and they have complicated forms that they are not suitable for the thin-ship assumption.

Although research in wave resistance has been a major interest among theoretical ship hydrodynamicists for almost a century it is not until recently that predictions, useful for arbitrary hulls, have become possible. A major breakthrough was the paper presented by **Dawson (1977)**. As had been suggested by **Gadd (1975)** the free surface boundary condition could be approximately satisfied by covering part of the undisturbed free surface close to the hull by sources. In Dawson's method the boundary condition is linear and the linearization is made about the so called double model solution, obtained assuming a flat free surface.

In this study the method which estimates a source distribution over the hull surface is used. The problem of steady flow about a ship is solved with the method which is based on simple Rankine singularities. The aim of the present work is to reduce the manual work required in preparing the input data for the programme which computes the wave-resistance.

Two pre-processor computer programmes are developed to automate data preparation for the main programme, namely for DAWSON.FOR developed previously at İ.T.Ü. by **Dr. Ömer Gören**. By using these pre-processor programmes different panel arrangements are tried both on the ship hull surface and on the free surface for Wigley's parabolic hull and Series-60 hull, respectively. By the two AutoCAD routines appended to these pre-processors it became possible to visualize the panel arrangements. The computed results are compared with the experimental results available.

ÖZET

DALGA DİRENCİ HESABI İÇİN GEMİ YÜZEYİNİN OTOMATİK OLARAK PANELLENMESİ

Gemi Hidrodinamiği alanında tekne formunun iyileştirilmesi önemli bir konudur. Tekne formu, geminin dalga yapıcı özelliklerini etkiler. Bu etkiler, yazında farklı birkaç yöntemle incelenmiştir. Dalga direnci problemlerinde kullanılan çözüm yöntemleri birkaç şekilde sınıflandırılabilir:

1) Tümlev (integral) denklem yöntemini kullanarak veya bilinen kaynak şiddetine sahip integrallerin doğrudan hesaplanması ile Green fonksiyonu yaklaşımı yapmak,

2) Sonlu farklar veya sonlu elemanlar yöntemlerinden birini kullanarak alan denklemlerinin doğrudan sayısal çözümlerini bulmak.

Green fonksiyonu yaklaşımı da, kullanılan Green fonksiyonuna göre iki sınıfa ayrılabilir:

a) Havelock (veya Kelvin) kaynaklarını kullanan yaklaşım,

b) Rankine kaynaklarını kullanan yaklaşım.

Havelock kaynakları daha çok narin gemi teorisinde (Thin Ship Theory) ve Neumann-Kelvin problemlerinde kullanılırken, Rankine kaynakları düşük hız teorisinde (Low Speed Theory) kullanılır.

Narin gemi teorisi birçok dalga problemine uygulanmıştır. Narin gemi yönteminde gemi formunu temsil eden eşdeğer kaynaklar gemi simetri ekseni üzerinde dağıtılır. Burada gemi genişliğinin gemi boyuna oranı çok küçük kabul edilir. Ancak inşaa edilen gemiler karmaşık forma sahip oldukları ve narin gemi kabulüne uygun olmadıkları için bu çalışmada gemi tekne formunun sadece gemi simetri ekseni üzerine dağıtılan kaynaklarla temsil edilmesinin uygun olmayacağı düşünülmüştür. Tekne yüzeyi üzerinde kaynak dağılımını öngören yöntem benimsenmiş, Rankine kaynaklarını kullanan yaklaşım kullanılmıştır.

Rankine kaynaklarında akım radyal doğrultuda dışa doğru bir akım olup, akım

hızı $1/r^2$ ile orantılıdır. Burada r kaynaktan olan uzaklıktır. Kaynağın kendisi dışında bu akım süreklilik (continuity) ve çevrisizlik (irrotationality) denklemlerini sağlar. Bu kaynaklar tekne yüzeyine dağıtılırsa, teknenin dışında viskoz olmayan bir akım oluşturulur. Kaynak dağılımı uygun olarak seçilirse, tekne yüzeyindeki sınır koşulu sağlanabilir. Pratikte bu sınır koşulu tekneyi N sayıda panele bölmekle başarılabilir.

Her bir panel üzerinde kaynak yoğunluğunun, σ_n gibi sabit bir değerde olduğu kabul edilir. Ancak σ_n panelden panele değişir. Teknenin ayna görüntüsü $z = 0$ serbest su yüzeyi düzlemi üzerine eklenir ve $\pm z$ noktalarındaki kaynak yoğunlukları birbirine eşit alınırsa, $z = 0$'daki düşey hız her yerde sıfır olur.

Uniform akım $\mathbf{V}$ ve N adet kaynaktan gelen etkinin birleştirilmesiyle oluşan bileşke hızın her bir panelin merkezine teğet olacağı kabul edilir. Bu kabul yardımıyla başlangıçta bilinmeyen N adet σ_n kaynak yoğunlukları bulunur.

Böyle bir akım, tekne sınır koşulunu sağlasa da serbest su yüzeyi koşulunu sağlamaz. Serbest su yüzeyi koşulunu sağlamak için $z = 0$ düzleminde ek paneller oluşturulur ve bu panellerin üzerine de Rankine kaynakları dağıtılır.

Serbest su yüzeyi katı (rijit) bir duvar kabul edilir. Elde edilen tümlev (integral) denklem tekne yüzeyi üzerine dağıtılmış kaynak yoğunluklarının fonksiyonu cinsinden sayısal olarak çözülür. Böylece tekne yüzeyindeki sınır koşulundan gemiyi temsil eden kaynak dağılımı tanımlanır.

Yapılan çalışmada kullanılan yöntemde gemi yüzeyi ve serbest su yüzeyi panellere ayrılır. Her bir panel üzerine tekillikler dağıtılır ve daha sonra bu dağılım tümlev denklemin çözümü olarak hesaplanır. Tümlev denklem olarak ikinci tip Fredholm tümlev denklemi kullanılmış ve kaynak yoğunluk dağılımı bu özel tümlev denklemin çözümü olarak elde edilmiştir.

Çalışmaya başlarken elimizde **Hess ve Smith (1966)** yöntemiyle hesaplama yapan bir bilgisayar programı bulunuyordu. DAWSON.FOR adlı bu ana program İ.T.Ü.'nde bf Dr. Ömer Gören tarafından geliştirilmiş bir programdır. Bu programa gerekli veriler (data) girildikten sonra gemi etrafındaki potansiyel akım ve dalga direnci, dalga bozulmaları (deformasyonları) gibi dalga özellikleri hesaplanmaktadır. Ancak programın veri dosyasını oluşturmak için gemi yüzeyinin ve serbest su yüzeyi-nin ve serbest su yüzeyinin elle panellenmesi, herbir panele ait köşe koordi-natlarının belli bir ölçekle çizilmiş gemi endazesi üzerinden ölçülmesi ve her bir köşeye bir numara atanması gerekmektedir. Veri dosyasını elle hazırlamak oldukça zaman alıcı ve ölçümlerin elle yapılması nedeniyle hatalara açık bir uygulamadır.

Elle bir kez panelleme yapmanın ve veri dosyası oluşturmanın alacağı zaman ve hata yapma olasılığının yüksekliği gözönünde bulundurulursa parametrik çalışma yapmanın güçlüğü ortaya çıkar. Veri dosyası hazırlamak kendi işler

(otomatik) hale getirilirse hata yapma olasılığı en aza ineceği gibi parametrik çalışma yapma olanağı da elde edilecektir.

Ana programa veri hazırlayan iki önişlemci (pre-processor) program geliştirilmiştir. Programlardan biri gemi yüzeyindeki panellere ait verileri hazırlarken diğeri serbest su yüzeyindeki panellere ait verileri hazırlamaktadır.

İlk veri dosyası gemi yüzeyi üzerindeki panellerin köşe konumları (koordinatları), köşe numaraları (indisleri) ve gemi boyu, gemi genişliği, su çekimi, boyuna yüzme merkezi gibi gemiye ait geometrik özelliklerden oluşmaktadır. İkinci veri dosyası ise serbest su yüzeyi üzerindeki panellerin köşe konumları ve köşe numaralarından oluşmaktadır.

Amaç elle yapılan veri dosyası hazırlama işlemini kendi işler (otomatik) duruma getirmek, böylece zamandan kazanç sağlamak ve ölçümler sırasında yapılabilecek hataları en aza indirmektir.

İlk dosyayı oluşturan programa APGOSH.FOR adı verilmiştir. Bu program veri dosyası olarak geminin ofset tablosunu kullanmaktadır. Program çalışırken kullanıcı istediği yere yeni su hatları, yeni postalar ekleyebilir ve istediği su hatlarını ve postaları çıkarabilir. İstenilen su hatları ve postaların kesişimi ile gemi yüzeyi üzerinde paneller elde edilir. Bunu yapabilmek için gemi yüzeyinin geometrik olarak tanımlanması gerekmektedir. Bu amaçla tiriz fonksiyonları (spline functions) kullanılmış, gemi su hatları ve postalarının konumları (koordinatları) bu fonksiyonlar yardımıyla geminin her yerinde tanımlanmıştır. Elde edilen panellerin köşe konumları birinci çıkış dosyasına yazdırılmıştır. Oluşturulan panellerin köşe numaraları da ana programın hesaplamasına uygun düşecek sırada, yani saat akrebinin dönüş yönünde, aynı çıkış dosyasına yazdırılmıştır.

İkinci dosyayı oluşturan program, APGOFS.FOR, serbest su yüzeyini belli bir bölgede sınırlandırır. Programın veri dosyası sınırlandırılmış bölgedeki ilk akım hattının konumundan oluşmaktadır. Program sınırlandırılmış serbest su yüzeyindeki ilk akım hattından yola çıkarak hayali akım hatları oluşturur. Tiriz fonksiyonları kullanılarak her bir akım hattının üçüncü dereceden (kübik) fonksiyonu elde edilmiştir.

Bu akım hatları gerçek akım hatları olmayıp, mühendislik yaklaşım sonucu oluşturulmuşlardır. Akım hatlarının veri dosyasında tanımlanan ilk akım hattına gemi ortasında paralel olduğu kabul edilmiştir. Baş ve kıç bölgeye gidildikçe iki akım hattı arasındaki uzaklığın artmasını sağlayacak geometrik bir yaklaşım yapılmıştır.

Akım hatları ile gemi simetri eksenine dik doğrular kesiştirilerek serbest su yüzeyinde de paneller oluşturulmuştur. Bu panellerin köşe noktalarının konumları da yine tiriz fonksiyonları yardımıyla hesaplanmıştır. Serbest su yüzeyindeki

panellerin köşe konumları ikinci çıkış dosyasına yazdırılmıştır. Serbest su yüzeyindeki panellerin köşe numaraları da ana programın hesaplamasına uygun düşecek şekilde, yani saat akrebinin dönüşüne aksi yönde ikinci veri dosyasına yazdırılmıştır.

APGOSH.FOR ve APGOFS.FOR önişlemcileri (preprocessors) ile oluşturulan iki ayrı çıkış dosyasının ana program tarafından okunabilmesi için ana program DAWSON.FOR içindeki giriş formatlarında bazı değişiklikler yapılmıştır.

Geliştirilen önişlemciler yardımıyla DAWSON.FOR adlı ana programın çalıştırılması için Wigley parabolik ve Seri-60 tekne formlarına ait veri dosyaları oluşturulmuştur.

Wigley tekne formuna ait dört ayrı veri dosyası oluşturulmuştur. Bu dört ayrı veri dosyası sırasıyla 194, 304, 388 ve 508 panelden oluşmaktadır. Oluşturulan veri dosyaları yardımıyla yapılan hesap sonuçları deneysel sonuçlarla karşılaştırılmıştır. Karşılaştırma sonunda panel sayısı arttıkça deneysel dalga direnci zarfının içinde kalan sonuçlar elde edildiği görülmüştür.

Ayrıca $Fn = 0.266$, $Fn = 0.348$ ve $Fn = 0.452$ Froude sayılarındaki dalga formları incelendiğinde panel sayısı arttırıldıkça deneysel verilere daha yakın sonuçlar elde edildiği görülmüştür.

Seri-60 formu için de farklı veri dosyaları oluşturulmuştur. Bu dosyaları kullanarak hesap yapıldığında dalga direnç katsayılarında ve çeşitli Froude sayılarına karşı gelen dalga formlarında deneysel verilerle bir benzerlik kaydedilmemiştir. Panel sayıları arttırılarak elde edilen sonuçlarda beklenen yakınsama görülmemiştir.

Hesaplamalar modelin sabit olduğu kabul edilerek yapılmıştır. Oysa deneysel veriler trim ve paralel batmaya serbest modeller için geçerlidir. Bu nedenle deneysel verilerle hesap sonuçlarının karşılaştırılması mertebe açısından çok gerçekçi değildir.

Her iki tekne için de sabit model deney verilerine ihtiyaç vardır. Wigley tekne formunda Froude sayısı arttıkça paralel batmanın dirence etkisi önem kazanmaktadır. Seri-60 tekne formu için de trim ve paralel batmanın dirence etkisi önemlidir. Seri-60 tekne formu için arabaya sabitlenmiş model deney verilerine ihtiyaç vardır.

Wigley formunda elde edilen sonuçların deneysel sonuçlarla uyumlu olmasına rağmen Seri-60 tekne formu için elde edilen hesap sonuçlarının deneysel verilerden çok uzaklaşması yapılan panellemede bir yaklaşım hatası olabileceğini düşündürmektedir. Bu hatanın iki nedenden kaynaklanabileceği düşünülmektedir. Bu nedenler şöyle sıralanabilir:

i) Tekne yüzeyi üzerindeki paneller su hatları ve postaların kesiştirilmesiyle oluşturulmuştur. Bu paneller yüzey eğriliğinin arttığı bölgelerde şekil olarak dikdörtgenden çok uzaklaşmaktadır. Eğer gemi yüzeyi üzerindeki paneller postalar ve postalara dik (ortogonal) eğriler kesiştirilerek oluşturulursa daha iyi sonuçlar elde edileceği düşünülmektedir. Ancak bu hatanın varlığı yürütülen çalışmanın belli bir aşamasından sonra ortaya çıktığından ayrılan süre içinde bu tür bir panellemenin otomatikleştirilmesi mümkün olmamıştır.

ii) Serbest su yüzeyindeki paneller gerçek akım hatları ve bunlara dik doğruların kesiştirilmesiyle değil, geometrik bir yaklaşım yapılarak oluşturulan hayali akım hatları ve bunlara dik doğruların kesiştirilmesiyle oluşturulmuştur. Bu ise serbest su yüzeyi üzerindeki sınır koşulunun tam olarak sağlanmasını engellemektedir. Gerçek akım hatları kullanıldığında yapılan hatanın ortadan kalktığı görülmüştür.

Yapılan çalışmanın çıkış noktası elle veri hazırlamanın ortaya çıkardığı güçlükler-di. Bu işin kendi işler duruma getirilmesi gerçekleştirilmiştir. Dört günlük bir iş 20 dakikalık bir hesaplama süresine indirilmiştir. Bunun, gemi dalga direnci problemleri alanında, sayısal hesaplama yöntemleriyle uygulamaya yönelik araştırma arasındaki boşluğu kapatmaya yönelik önemli bir adım olduğu düşünülmektedir.

CHAPTER 1. INTRODUCTION

The improvement of a ship hull form is a recent development in the field of ship hydrodynamics. The ship hull form affects the wave-making characteristics of the ship. These effects have been explored by using different theories. One of these theories is the thin ship theory. The thin ship theory has been applied for almost all wave-making problems. However, almost all real ships are not so thin and they have complicated forms that they are not suitable for the thin ship assumption. In the method of the thin ship theory the equivalent sources representing ship form is distributed on the centerplane of a ship on the assumption that the breadth of the ship is very small in comparison with its length. Therefore we found that it is not suitable to represent the ship hull form only by the source distribution on the centerplane of the ship. Hence, the method which estimates the source distribution over the hull will become remarkable.

From the boundary condition at the hull surface we can determine the surface source distribution representing the ship by assuming the free surface to be a rigid wall and by solving numerically the integral equation for the function of source density distributed over the hull surface as **Hess and Smith (1966)** did.

The method described in this work utilizes a distribution of singularity over the body surface and computes this distribution as the solution of an integral equation. Specifically, a source density distribution is obtained as the solution of a Fredholm integral equation of the second kind. The method is numerically exact in sense that any degree of accuracy may be obtained.

1.1. Background and Previous Work

A number of numerical methods for computing free-surface flows about ship forms are presented as robust and accurate on the basis of favourable comparisons between numerical predictions and experimental measurements.

In particular, a number of numerical methods are known to yield predictions that can be quite sensitive to the panelization of the ship hull. Mainly two classes of numerical methods are used for predicting steady flow about a ship, namely: methods based on simple Rankine singularities, which were initiated by **Gadd (1976)**, **Dawson (1977)** and **Daube (1980)** and have since been quite popular, and methods based on Kelvin-Havelock singularities, which satisfy the linearized free-surface boundary condition. The latter group of methods offer several important advantages, notably; panels are required only on the hull surface not on the free-surface, the radiation condition is satisfied automatically and exactly.

Kelvin singularity predictions were generally found superior to Rankine singularity predictions in **Lindenmuth et al.(1991)**. However, the popularity of Rankine singularity methods relative to Kelvin singularity methods can be largely attributed to the complexities of the latter one.

In wave resistance problems, solution of the double-model by the panel method had become possible only after **Dawson (1977)** had developed a differentiation scheme satisfying the free-surface condition and introduced the related numerical algorithm.

Baba and Hara (1977) searched for a solution by distributing singularities on the ship surface. **Gadd (1976)** and **Çalışal et al.(1991)** used iterative methods for the solution. **Nakatake et al.(1991)** based on Dawson's formula, distributed doublets on the body surface. **Cheng (1989)** made an additional improvement to the wave making problem of dry transom ships by utilizing new kinematic conditions at the transom in Dawson's method.

1.2. Present Work

A lot of manual work is required to prepare input data for the programme DAWSON.FOR developed previously at İ.T.Ü. by **Dr. Ömer Gören** which computes wave-making characteristics of ships, namely, the wave resistance, heave force and trim moment. To reduce this manual work which 80% of the time is spent on, two computer programmes are developed. These programmes can be accepted as preprocessors for the main programme DAWSON.FOR. The preprocessors are used to prepare the input data for two hull forms: Wigley's

Parabolic Hull and Series-60 Hull forms, respectively. By using automatically generated input data, programme DAWSON.FOR is run for different number of panels and panel arrangements. The effects of the increment in the number of panels on the accuracy of the computed results are examined by comparing these results with experimental data.

By increasing the number of panels more accurate results are obtained while much computing time is required. An optimum number of panels is searched that will both give compatible results with experimental data and take minimum computing time.

Fundamental equations of Dawson's Method and the method of solution of the integral equations are given in **Chapter 2.** A brief history of mesh generation scheme is given in **Chapter 3.** Also computer defined surface elements and Spline Functions which form the basis of the pre-processor programmes' algorithm are thoroughly defined in **Chapter 3.** Description of the pre-processor programmes used in this study is given briefly in **Chapter 4.** Comparison of computed and experimental results for both the Wigley's Parabolic and the Series-60 hull forms are shown graphically in **Chapter 4.** Concluding remarks and suggestions for future work are given in **Chapter 5.** Offset data and drawings of the two hull forms are given in **Appendix A** and **Appendix B.**

CHAPTER 2. THE FUNDAMENTAL PROBLEM

2.1. Definition of Potential Flow

Let V denote the fluid velocity at any point, p the fluid pressure, and ρ the constant fluid density. If the viscosity is set equal to zero and the density is taken as constant, the general Navier-Stokes equations reduce to the well-known Eulerian equation of motion

$$\frac{\partial \mathbf{V}}{\partial t} + (\mathbf{V} \cdot grad)\mathbf{V} = -\frac{1}{\rho} grad\ p \tag{2.1}$$

and the equation of continuity becomes

$$div(\mathbf{V}) = 0 \tag{2.2}$$

Equations (2.1) and (2.2) hold in the field of flow, the region exterior to the boundary surfaces. This region will be denoted R' as can be seen from **Figure 2-1.**

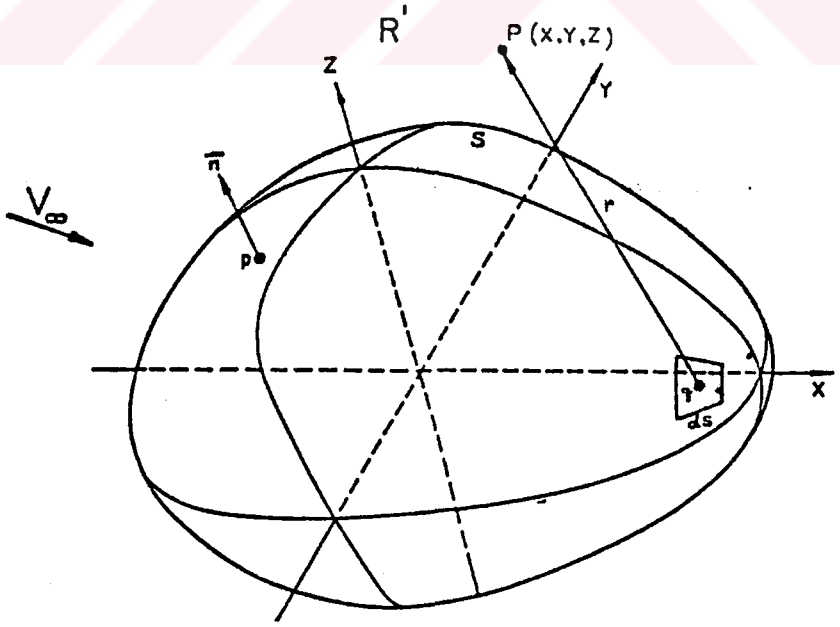

Figure 2-1. Flow about a three dimensional body surface

Certain boundary conditions must be added to these equations. The location of all boundary surfaces are assumed known, possibly as functions of time, and

the normal component of fluid velocity is prescribed on these boundaries. The entire boundary will be denoted by S (S is the boundary of the region R'), and the boundary condition will be written as

$$\mathbf{V} \cdot \mathbf{n}|_s = F \tag{2.3}$$

where $\mathbf{n}$ is the unit outward normal vector at a point of S, and F is a known function of position on S and possibly also a known function of time. For the exterior problem a radiation condition at infinity must also be imposed. In deriving the equations of potential flow it is assumed that the velocity field $\mathbf{V}$ is irrotational and that it can therefore be expressed as the negative gradient of a scalar potential function Φ. It includes all flows that can be generated from rest by the action of conservative body forces or by the motion of the boundaries. A slightly more general class of flows will be considered in this work. The velocity field $\mathbf{V}$ is expressed as the sum of two velocities:

$$\mathbf{V} = \mathbf{V}_\infty + \mathbf{v} \tag{2.4}$$

The vector $\mathbf{V}_\infty$ is the velocity of the onset flow, which is defined as the velocity field that would exist in the fluid if all boundaries ceased to exist or if all boundaries became simply transparent with regard to fluid motion. The vector $\mathbf{v}$ is the disturbance velocity field due to the boundaries. The velocity $\mathbf{v}$ is assumed to be irrotational, but $\mathbf{V}_\infty$ is not so restricted. Accordingly, $\mathbf{v}$ may be expressed as the negative gradient of a potential function φ, that is,

$$\mathbf{v} = -grad\ \varphi \tag{2.5}$$

Since $\mathbf{V}_\infty$ and $\mathbf{v}$ are the velocities of an incompressible flow, they satisfy Eq.(2.2); that is,

$$div(\mathbf{v}) = 0 \tag{2.6}$$

Using $\mathbf{v}$ from Eq.(2.5) in Eq.(2.6) then gives the potential φ that satisfies Laplace's equation,

$$\nabla^2 \varphi = 0 \tag{2.7}$$

in the region R'. The boundary conditions on φ arise from equations (2.3),(2.4), and (2.5) in the form

$$grad\ \varphi \cdot \mathbf{n}|_s = \frac{\partial \varphi}{\partial n}|_s = \mathbf{V}_\infty \cdot \mathbf{n}|_s - F \tag{2.8}$$

In the usual exterior problem the radiation condition is

$$|grad\ \varphi| \to 0 \tag{2.9}$$

at infinity. Equations (2.7), (2.8), and (2.9) comprise a well-set problem for the potential φ, and it is this problem that the method of this work is designed to solve.

The onset flow $\mathbf{V}_\infty$ must be such that the disturbance velocity $\mathbf{v}$ is a potential flow. In the usual case, when $\mathbf{V}_\infty$ is also a potential flow, this condition is obviously satisfied.

The essential simplicity of potential flow derives from the fact that the velocity field is determined by the equation of continuity, Eq.(2.6), and the condition of irrotationality, Eq.(2.5). Thus the equation of motion, Eq.(2.1) is not used, and the velocity may be determined independently of the pressure. Also the time, t, enters only as a parameter in Eq.(2.8); therefore the instantaneous velocity is obtained from the instantaneous boundary condition; that is, all problems are essentially steady with respect to determination of the velocity. Once the velocity field is known, the pressure is calculated from Eq.(2.1). The only cases of interest are those for which Eq.(2.1) can be integrated to give one of the forms of the Bernoulli equation. When $\mathbf{V}_\infty$ is a potential flow, so that the combined velocity field is $\mathbf{V} = -grad\Phi$, then Eq.(2.1) integrates to

$$\frac{p}{\rho} = P(t) - \frac{1}{2}|\mathbf{V}|^2 + \frac{\partial \Phi}{\partial t} \qquad \textbf{(2.10)}$$

Where $P(t)$ is independent of position in the field. In most applications the flow is steady, and the onset flow is a uniform stream, that is, $\mathbf{V}_\infty$ is a constant vector. Under these circumstances Eq.(2.10) can be written in terms of the pressure coefficient C_p as

$$C_p = \frac{p - p_\infty}{\frac{1}{2}\rho|\mathbf{V}_\infty|^2} = 1 - \frac{|\mathbf{V}|^2}{|\mathbf{V}_\infty|^2} \qquad \textbf{(2.11)}$$

where p_∞ is the pressure at infinity.

The problem defined by the equations (2.7), (2.8), and (2.9) is seen to be a classic Neumann problem of potential theory. But the fluid-dynamics problem has certain special features that distinguish it from the fully general Neumann problem. In particular, the usual problem is the exterior one, so that the domain of the unknown φ is infinite in extent; but often the solution is of interest only on the boundaries.

The above formulation is quite general, including as it does cases of unsteady nonuniform onset flows, ensembles of bodies with nonrigid surfaces moving with respect to each other, internal flows, and area suction on the boundaries. The method can be generalized to solve other simple, linear, homogeneous, elliptic partial differential equations. But the method fails in solving certain classes of potential-flow problems such for which the location of part of the boundary is unknown.

The neglect of viscosity is justified except at points in or very near regions of catastrophic separation, for example, wakes. Local regions of separation and reattachment do not normally invalidate the calculations. The neglect of compressibility is justified for all flows where the local Mach number does not exceed a value of approximately one-half. By suitably adjusting the calculations, the validity can be extended up to a local Mach number of unity. That is, the adjusted calculated flow agrees with real flow as long as there are no supersonic regions.

2.2. Evaluation of the Integral Equation for A Source-Density Distribution On The Body Surface

The exact solution of the direct problem of potential flow for arbitrary bodies can be approached in a variety of ways, all of which must finally become numerical and make use of a computing machine. The method of this work is based on an integral equation for a source-density distribution on the surface of the body or bodies about which the flow is being computed.

The problem considered is that defined by equations (2.7), (2.8), and (2.9). A sketch illustrating the situation for a single three-dimensional body is shown in **Figure 2-1.** A unit point source is located at a point q whose Cartesian co-ordinates are x_q, y_q, z_q. At a point P whose co-ordinates are x, y, z the potential due to this source is

$$\varphi = \frac{1}{r(P,q)} \tag{2.12}$$

where $r(P,q)$ is the distance between P and q, namely,

$$r(P,q) = \sqrt{[(x-x_q)^2 + (y-y_q)^2 + (z-z_q)^2]} \tag{2.13}$$

The potential (2.12) gives rise to a velocity radially outward in all directions from the point q, and thus the point q may be thought of as the location of a *source* of fluid. The solution is built up of elementary potentials of the form Eq.(2.12). The potential in Eq(2.12) satisfies Eq.(2.9) and Eq.(2.7) at all points except the point q. Because of the linearity of the problem, the potential due to any assembles of such sources or any continuous distribution of them that lies entirely interior to or upon the boundary surface S satisfies Eq.(2.9) and Eq.(2.7) in the region R' exterior to S. If the local intensity of the distribution is denoted by $\sigma(q)$, where the source point q now denotes a general point of the surface S as seen from **Figure 2-1**, then the potential of the distribution is

$$\varphi = \iint_S \frac{\sigma(q)}{r(P,q)} dS \tag{2.14}$$

Regardless of the nature of the function $\sigma(q)$, the disturbance potential as given by Eq.(2.14) satisfies two of the three equations of the direct problem of potential flow. This function is determined from the requirement that the potential also must satisfy the other equation, Eq.(2.8), which expresses the normal velocity boundary condition on the surface S. Applying the boundary condition, Eq.(2.8), as well as subsequently evaluating fluid velocity on the surface, requires evaluating the limits of the spatial derivatives of Eq.(2.14) as the point P approaches a point p on the surface S. Care is required because the derivatives of $1/r(P,q)$ become singular as the surface is approached.

In accordance with the procedure presented by **Kellogg (1929)**, the disturbance potential as given by Eq.(2.14) is differentiated, and the boundary condition, Eq.(2.8), applied to it by allowing the point P to approach a point p on the surface S. The result is the following integral equation for the source-density distribution $\sigma(p)$:

$$2\pi\sigma(p) - \iint_S \frac{\partial}{\partial n}\Big(\frac{1}{r(p,q)}\Big)\sigma(q)dS = -\mathbf{n}(p)\cdot\mathbf{V}_\infty + F \tag{2.15}$$

where $\partial/\partial n$ denotes differentiation in the direction of the outward normal to the surface S at the point p, and the unit outward normal vector $\mathbf{n}(p)$ depends on location. The solution of Eq.(2.15) is the central problem of the present method.

Equation (2.15) is a Fredholm integral equation of the second kind over the boundary surface S. The term $2\pi\sigma(p)$ arises from the delta function that is

brought in by the limiting process of approaching the boundary surface. The kernel of the integral equation, $-\partial/\partial n[1/r(p,q)]$, is the outward normal velocity at the point p due to a unit point source at the point q. This kernel depends only on the geometry of the surface S. The theory of the solution of Eq.(2.15) is discussed by **Kellogg (1929)** and fundamental existance and uniqueness theorems are presented. The conditions under which a solution can be obtained are very general. The surface S need not be slender or analytic. In fact, for the flow exterior to a given surface, S may consist of several disjoint surfaces. Internal flows as well as external may be considered. There is one restriction on Eq.(2.15). The existance proof of Kellogg requires that the right side of Eq.(2.15), be a continuous function of position on the surface. This means that in general the surface S must have a continuous normal vector. Thus boundaries with corners are excluded from the existance proof. In practice, however, it has been found that the present method does give correct results near convex corners, where the surface velocity is in general infinite. For concave corners the method has difficulty, especially if the corner is a stagnation point of the flow. For some onset flows or for corners of small turning angle, the calculated results are sufficiently accurate for most purposes. Other situations require the concave corner to be rounded in order to obtain an accurate solution.

For a known boundary surface S, the kernel of Eq.(2.15) can be calculated in a straightforward manner, and the equation is a linear one for the unknown function σ. The only possibility of using the present method for problems having boundaries with unknown locations is to assume the locations of all boundaries, solve the resulting direct problem, and then repeat the process after adjusting the boundaries by *cut and try* until all conditions are satisfied.

Equation (2.15) is an integral equation of the second kind, for which the unknown function appears outside the integral as well as inside. Equations of the second kind have many advantages, both theoretical and practical. Numerically, integral equations of the second kind are considerably more tractable. If the integral equation is approximated by a set of linear algebraic equations, as it is in the present method, the presence of the term outside the integral insures that in general the diagonal entries of the resulting coefficient matrix will be much larger than any off-diagonal entries. This property can be crucial numerically if iterative matrix-solution methods are used.

The term $2\pi\sigma(p)$ on the left side of Eq.(2.15) is the contribution to the out-

ward normal velocity at a point p on the boundary of the source-density in the neighbourhood of P. The integral term represents the contribution of the source-density on the remainder of the boundary surface to the outward normal velocity at p. To illustrate the magnitude of these terms the source-density will be assumed to have a constant value of unity over the boundary surface S. The normal velocity in the direction exterior to S at a point p due to this source distribution is given by the left side of Eq.(2.15) as

$$[V_n(p)]_{\sigma=1} = 2\pi - \iint_S \frac{\partial}{\partial n}\Big(\frac{1}{r(p,q)}\Big)dS \qquad \textbf{(2.16)}$$

If this expression is integrated over the entire closed surface S, the result is the total velocity flux outward from S due to the source distribution. From the definition in Eq.(2.14) it is seen that the total velocity flux due to a unit point source is 4π. Thus the total flux due to a unit source distribution on S is 4π times the total surface area S. If Eq.(2.16) is integrated over S, the local contribution given by the first term on the right is 2π times the total surface area of S. Thus the integral over S of the second term on the right side of Eq.(2.16) is exactly equal to that of the first term.

There is a certain difference between the exterior flow problem and the interior flow problem. If the same closed surface is considered, the only difference between the two problems is the reversal of the outward normal direction n and thus the reversal of the sign of the integral term of Eq.(2.15). If the boundary surface is convex, the kernel of Eq.(2.15) is positive for the exterior problem and negative for the interior one. For the exterior problem, the integral equation is determinative in that if the right side of Eq.(2.15) is zero, the only solution is $\sigma = 0$; that is, no nonzero source distribution gives rise to zero normal velocity everywhere on the boundary. Thus the solution of the exterior problem exists and is unique, and no difficulties are encountered in solving the equation. For the interior problem the integral equation (2.15) is indeterminative; that is, there is a source distribution, not identically zero, that gives zero normal velocity everywhere on the boundary. Clearly such a source distribution gives zero fluid velocity everywhere within the boundary. Thus a source-density distribution for the interior problem exists only if the right side of Eq.(2.15) satisfies a certain condition, and if it does exist, it is not unique. The condition required of the right side is that its integral over the boundary must vanish. This simply means that the total flux across the boundary must be due to the onset flow, for example, due to interior sources. The surface source-density distribution does

not contribute to the flux. This is certainly a physical requirement for flow of an incompressible fluid.

If the integral equation is approximated by a set of linear algebraic equations, the coefficient matrix for the interior problem is either singular or nearly singular, depending on the details of approximation. In the present method the matrix is nearly singular, and nothing unusual seems to occur in the calculations.

2.3. The Method of Solution

The method chosen for the numerical solution of the integral equation,Eq.(2.15) was dictated, to a considerable extent, by the fact that the boundary surface S, which is the domain of integration, is completely arbitrary. This means that the integration must be performed numerically rather than analytically, as the methods that approximate the kernel of the unknown function by a series of suitably chosen functions that are not very attractive. Two approaches present themselves. The equation may be attacked directly as an integral equation by using an iterative procedure appropriate for Fredholm Integral equations. Alternatively, the integral equation may be approximated by a set of linear algebraic equations, which are solved by any of the usual techniques. In the former, the integral is evaluated by some form of approximate quadrature, and the process is iterated. In the latter, an approximate quadrature, is used to obtain a set of linear equations, which may then be solved by iteration. For either approach an approximate integration procedure must be selected from among the large number of available quadrature formulas. Here, the fact that the boundary is arbitrary affects the situation. This surface must be approximated in some manner for the computer, and the manner of approximating the surface is bound up with the approximate integration procedure, as it is with the entire method of solution.

2.4. Present Approach

The approach adopted consists of approximating Eq.(2.15) by a set of linear algebraic equations. The boundary or body surface S about which the flow is to be computed is approximated by a large number of surface elements, whose characteristic dimensions are small compared to those of the body. Over each

surface element the value of the surface source-density is assumed constant. This reduces the problem of determining the continuous source-density function σ to that of determining a finite number of values of σ, one for each of the surface elements. The contribution of each element to the integral in Eq.(2.15), can be obtained by taking the constant but unknown value of σ on that element out of the integral and then performing the indicated integration of known geometric quantities over the element. Requiring the normal velocity to take on its prescribed value at one point, gives a linear relation between the values of σ on the elements. On each element a control point is selected where Eq.(2.15) is required to hold. This gives a number of linear equations equal to the number of unknown values of σ. The coefficient matrix consists of the normal velocities induced by the elements at each other's control points for unit values of source-density. Once the linear equations have been solved, flow velocities and potential may be calculated at any point by summing the contributions of the surface elements and that of the onset flow. Usually, velocities and pressures on the body surface are of greatest interest. Because of the manner in which the solution has been effected, these must be evaluated at the control points, that is, at the same points where the normal velocity was made to assume its prescribed value.

2.5. Approximation of the Body by Surface Elements

The basic input to the computer program consists of the specification of

(i) the body surface about which the flow is to be computed,

(ii) the onset flow if this is not a uniform stream,

(iii) the prescribed normal velocity on the surface if this is not zero.

Of several possible ways of specifying the body surface, the only one seriously considered consists in defining the body by means of the co-ordinates of a set of points distributed over the surface. The numerical significance of the co-ordinates of the input points must be sufficient to guarantee the accurate computation of surface slopes. Because the input points are used to form the approximating surface elements, their distribution and total number determine the accuracy of the resulting calculations.

Figure 2-2. shows the surface elements used to approximate three-dimensional bodies. For two dimensional and axisymmetric body shapes, only a single profile curve need to be defined by input points. This curve is assumed to lie in the xy-plane, and the x-axis is always taken as the symmetry axis for axisymmetric bodies. For closed two-dimensional bodies, a complete closed curve is specified by input points, and an axisymmetric closed body is specified by input points lying on the half of the contour in the half-plane $y \geq 0$. These points are connected by straight-line segments, and the profile curve is approximated by an inscribed polygon. The surface elements for two dimensional bodies are thus thin, infinite plane strips, and those for axisymmetric bodies are frustums of cones having small slant height. For truly three-dimensional bodies, the input points must be distributed over the entire surface. These points are associated in groups of four and used to form plane quadrilateral surface elements as shown in **Figure 2-2**. The plane of the element is equidistant from the four input points used to form it, and its normal vector $\mathbf{n}$ is the normalized cross-product of two *tangential* vectors each of which is obtained by subtracting the co-ordinates of two of the four input points. The corners of the quadrilateral are projections of the four input points into the plane of the element. In forming these elements, most input points are used in the formation of four elements, so that the number of input points required is only slightly larger than the number of resulting elements.

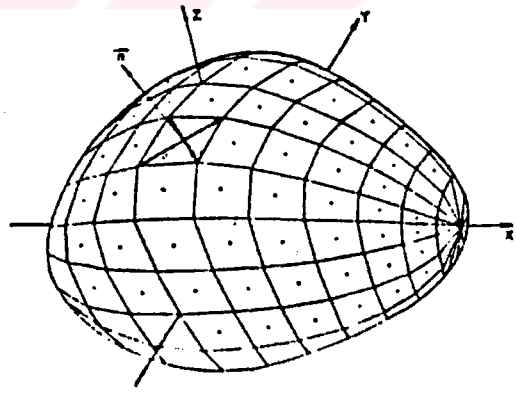

Figure 2-2. Approximation of the body surface by elements

For all body geometries, the order in which the points defining the surface are input determines which direction is considered the *outer* normal direction and thus determines on which side of the surface the flow is computed. In the case of exterior flow about a single closed contour, the defining points are input in clockwise order about the contour. If an interior flow is desired, the points are

input in counter-clockwise order.

On each element a control point is selected at which the normal velocity boundary condition is to be satisfied. For two-dimensional and axisymmetric bodies, the control points are the midpoints of the line segment joining the input points that define profile curve. On each quadrilateral element there is one point at which a constant source-density on that element gives rise to no velocity in the plane of the element; that is, there is a point at which the effect of the element is entirely normal. It was decided to use this point as the control point, although subsequent results indicated that the centroid of the area of the quadrilateral is an equally good choice. These two points are not necessarily near each other if the element is not approximately rectangular.

It should be emphasized that for all body geometries the surface elements are simply devices for effecting the numerical solution of the integral equation (2.15). They essentially define integration increments and normal directions at points of the surface. At the edges of the elements the velocity approaches infinity because of the discontinuity of the source-density and/or the discontinuity in slope, but the approach to infinity is not that associated with corner flows. The computed flow has significance only at the control points themselves and at points off the body surface.

From the manner in which quadrilateral elements are formed in three-dimensional cases, it is evident that in general the edges of adjacent elements are not coincident; that is, there are small *openings* between the elements. Any errors due to this source are of higher order than, and are negligible compared to, those due to the basic approximation of the body surface by plane elements over each of which the source-density is constant.

2.6. The Effects of the Elements at Each Other's Control Points

Once the body surface has been approximated by elements of the appropriate type, the elements are ordered sequentially and numbered from 1 to N, where N is the total number of elements. The exact order of the sequence is immaterial. Reference will accordingly be made to the ith element and the jth element, where the integers i and j denote the positions of the elements in the sequence.

Assume for the moment that the surface source-density on the jth element has the constant value of unity. Denote by Φ_{ij} and $\mathbf{V}_{ij}$ the potential and velocity, respectively, that are induced at the control point of the ith element by a unit source-density on the jth element. The formulas for the induced potential and velocity form the basis of the present method of flow calculation. They are obtained by integrating over the element in question the formulas for the potential and velocity induced by a unit point source and thus depend on the location of the point at which the potential and velocity are being evaluated and also on the geometry of the element. Since there is no restriction on the location of the control point of the ith element with respect to the jth element, the formulas for Φ_{ij} and $\mathbf{V}_{ij}$ are those for the potential and velocity induced by an element at an arbitrary point in space. The dependence of the formulas on the geometry of the element means that there are three distinct sets of formulas for Φ_{ij} and $\mathbf{V}_{ij}$, corresponding to the three different types of elements that are appropriate for use with two-dimensional bodies, and fully three-dimensional bodies, respectively.

2.7. Three Dimensional Flow

For the plane quadrilateral elements used to approximate three-dimensional bodies, the unit-point-source formulas for potential and velocity can be integrated analytically over an element. This is most conveniently done by using a co-ordinate system in which the element itself lies in a co-ordinate plane, and thus co-ordinates of points and components of vectors must be transformed between the reference co-ordinate system in which the body surface is input and an *element co-ordinate system* based on the element in question. The analytic integration over the element produces rather lengthy formulas, whose evaluation is time consuming. To conserve computing time, the effect of an element at points sufficiently far from the element is calculated approximately. This is accomplished by means of multipole expansion. In fact, if the point in question is farther from the centroid of the element than four times the maximum dimension of the element, the quadrilateral source element may be replaced by a point source of the same total strength located at its centroid. With the accuracy criteria adopted, errors due to the use of the multipole expansion or point-source formulas are apparently small compared with those arising from the basic approximation of the body surface by plane elements having constant values of source-density.

When this phase of the calculation has been completed, the result consists of the $N \times N$ matrices Φ_{ij} and $\mathbf{V}_{ij}$ that give the potentials and velocities induced by the elements at each other's control points for a unit source-density. The details for the calculation of $\mathbf{V}_{ij}$ and Φ_{ij} can be found in **Hess and Smith (1966)**. The vector matrix $\mathbf{V}_{ij}$ is

$$\mathbf{V}_{ij} = X_{ij}\mathbf{i} + Y_{ij}\mathbf{j} + Z_{ij}\mathbf{k}, \tag{2.17}$$

where **i**, **j**, **k** are the unit vectors along the axes of the reference co-ordinate system in which the body surface is input, and the scalar matrices X_{ij}, Y_{ij}, Z_{ij} are simply the components of $\mathbf{V}_{ij}$. The normal velocity induced at the control point of the ith element by a unit source-density of the jth element is

$$A_{ij} = \mathbf{n}_i \cdot \mathbf{V}_{ij}, \tag{2.18}$$

where $\mathbf{n}_i$ is the unit normal vector to the ith element. The five matrices Φ_{ij}, X_{ij}, Y_{ij}, Z_{ij}, and A_{ij} do not necessarily have any zero entries. The number of elements used in three-dimensional cases is large enough for the handling of the amount of numerical data represented by these matrices to be a considerable problem.

The $i = j$ case does not require special handling. The velocity induced by an element at its own control point has a magnitude of 2π and is directed along the element's normal vector.Once the potential and velocity induced at the control point of the ith element by the jth element has been computed, the jth element is reflected in each symmetry plane and the calculation repeated. The effects of the reflected elments at the control point of the ith element are either added or subtracted from the effect of the jth element itself, depending on whether the pertinent plane is one of symmetry or antisymmetry. Thus although potentials and velocities induced by elements all over the body surface must be computed, they are computed only at control points on the nonredundant portion and are added, so that the matrices Φ_{ij} and $\mathbf{V}_{ij}$ have an order equal to the number of elements describing the nonredundant portion of the body surface.

2.8. Approximation of the Integral Equation By A Set of Linear Algebraic Equations

A result of the calculation discussed in the previous section is the matrix A_{ij}, whose entries are the normal velocities induced by the elements at each other's

control points for unit values of source-density. To obtain actual normal velocities, the entries of A_{ij} must be multiplied by the proper values of the source-density σ. In particular, the quantity

$$\sum_{j=1}^{N} A_{ij}\sigma_j \tag{2.19}$$

is the normal velocity at the control point of the ith element due to complete set of surface elements. Clearly Eq.(2.19) is the approximation of the normal velocity associated with the disturbance potential of the body surface. To obtain the prescribed normal velocities at the control points of all elements Eq.(2.19) must be set equal to the proper value as given by Eq.(2.8) for every value of i. The result is

$$\sum_{j=1}^{N} A_{ij}\sigma_j = -\mathbf{n}_i \cdot \mathbf{V}_{\infty i} + F_i, \qquad i = 1, 2, ..., N. \tag{2.20}$$

Equation (2.20) is a set of linear algebraic equations for the values of source-density on the surface elements. This set of linear algebraic equations is the desired approximation of the integral equation, Eq.(2.15).

Both direct and iterative methods are used for solving Eq.(2.20) for the set of source-densities σ_j. Normally, an iterative solution is used for three dimensional flows. In the usual case, the onset flow velocity $\mathbf{V}_\infty$ is simply a constant vector of unit magnitude, and the prescribed normal velocity F is zero. In such a case, the points on the body surface are the only input to the method.

For a given type of flow the matrix A_{ij} (and all other computed matrices) depends only on the geometry of the body surface and is independent of the onset flow or prescribed normal velocity. A two-dimensional body has only one A_{ij} for all flows. The same is true for a three-dimensional body if symmetry is not utilized or if all onset flows have the same symmetry. An axisymmetric body has one A_{ij} for all symmetric flows and another one for all cross flows.

2.9. Computation of the Flow Quantities of Interest

Once the values of the source-density σ_j have been obtained as the solution of Eq.(2.20) all other flow quantities of interest can be obtained by relatively a rapid direct calculation. Flow quantities on the body surface are computed

only at the control points of the elements by use of the matrices described in **Section 2.7.**

In three-dimensional cases, the potential and velocity at a control point on the body surface are calculated from

$$\begin{aligned} \varphi_i &= \sum_{j=1}^{N} \Phi_{ij}\sigma_j \\ \mathbf{V}_i &= \sum_{j=1}^{N} \mathbf{V}_{ij}\sigma_j + \mathbf{V}_{\infty i} \end{aligned} \qquad i = 1, 2, ..., N. \tag{2.21}$$

The velocity $\mathbf{V}_i$ at each control point is given in terms of its components along the axes of the reference co-ordinate system in which the body is input. In actual computation, the scalar matrices X_{ij}, Y_{ij}, and Z_{ij} are multiplied by σ and summed. Notice that φ_i is the perturbation potential due to the body surface, and $\mathbf{V}_i$ is the total velocity, including the effects of the onset flow. The components of $\mathbf{V}_i$ are used to compute velocity magnitude and then pressure coefficient from Eq.(2.11). The latter quantity has meaning only for a uniform onset flow.

Flow quantities may be computed at points off the body surface for all flow geometries. The co-ordinates of an off-body point are input and used to obtain quantities Φ_{ij} and $\mathbf{V}_{ij}$ for $j = 1, 2, ..., N$. These are calculated by the same formulae as those used for calculating induced potential and velocity at a control point of a surface element. It is simply a matter of using the co-ordinates of the off-body point in place of the co-ordinates of the ith control point. The potential and velocity at such a point are calculated in the form

$$\begin{aligned} \varphi &= \sum_{j=1}^{N} \Phi_{ij}\sigma_j \\ \mathbf{V} &= \sum_{j=1}^{N} \mathbf{V}_{ij} \cdot \sigma_j \end{aligned} \tag{2.22}$$

(the use of the subscript i on Φ_{ij} and $\mathbf{V}_{ij}$ is perhaps misleading in this context, since the computation is at an off-body point, not at the control point of the ith surface element. The subscript has been retained to avoid introducing another symbol for a quantity that is calculated in exactly the same way as it is for

points on the body surface. Perhaps i can be thought of here as denoting the ith off-body point.) At off-body points both the potential and velocity are perturbation quantities due only to the effect of the body surface, unless the onset flow is a uniform stream, in which case its effect can be added to the velocity. For all flow geometries, the velocity at off-body points is given by its component along the axes of the reference co-ordinate system.

CHAPTER 3. MESH GENERATION AND SPLINES

The area of numerical grid generation is relatively young in practice, although its roots in mathematics are old. This somewhat eclectic area involves the engineer's feel for physical behaviour, the mathematician's understanding of functional behaviour, and a lot of imagination.

Numerical grid generation can be thought of as a procedure for the orderly distribution of observers, or sampling stations, over a physical field in such a way that efficient communication among the observers is possible and that all physical phenomena on the entire continuous field may be represented with sufficient accuracy by this finite collection of observations. The structure of an intersecting net of families of co-ordinate lines allows the observers to be readily identified in relation to each other, and results in much more simple coding than would the use of a triangular structure or a random distribution of points.

Computer-oriented mesh generators, which serve as pre-processors to finite element programs, have recently been developed by several investigators to alleviate the frustration and to reduce the amount of time involved in the tedious manual subdividing of a complex structure into finite elements (or meshes).

The conventional finite element method (FEM) involves the partitioning of a polygonal domain into rectangular, and/or triangular elements. Quite often, however, a structural engineer is faced with a boundary value problem over a nonpolygonal domain, which in fact is the case in the potential flow problem around a ship hull.

In order to better conform to curved boundaries and material interfaces, curved finite elements have been widely applied in recent years by practicing engineering analysts. The most well known of such elements are the *isoparametric elements*. As **Zienkiewicz (1971)** points out there has been a certain parallel between the development of element types as used in finite element analysis and the independent development of methods for the mathematical description of general free-form surfaces.

Whether rectangular,triangular, isoparametric, transfinite or whatever other elements are to be used, the basic problem of where to place the nodes or mesh points must first be solved. If done manually, this involves a considerable expenditure of time and almost invariably results in a mesh for which a natural ordering of the nodes may not be apparent. In this work an approach to automatic mesh generation based upon a systematic and unified class of schemes for treating the geometric aspects of the finite element method is used. We refrain from calling the technique *automatic* mesh generators since the actual problem of mesh definition must ultimately be resolved by the analyst who is cognizant of his specific application; that is , mesh generation involves both geometry and physics and in this work we consider only the geometric aspects.

3.1. Previous Work

In recent years irregular computational grids have become increasingly popular for a wide variety of numerical modelling applications. This trend demonstrates widespread appreciation of the two computational advantages that irregular grids can provide: they allow points to be situated on curved boundaries of irregularly shaped domains. On the other hand, anyone who wants to use an irregular grid must take on the task of grid construction, which can demand as much attention and effort as the computation for which the grid is intended.

There is an alternative to computing with irregular grids. A co-ordinate transformation can be used to map a geometrically irregular computational domain into a more regular one for which a uniform grid is appropriate. After solving transformed equations on a regular grid in the transformed domain, the inverse transformation can be used to map the solutions back into the original, irregular domain. The disadvantage of this alternative approach is that an appropriate co-ordinate transformation must be prescribed before computations begin. The task of specifying this transformation is quite similar to that of constructing an irregular grid. In fact, the inverse transformation maps the regular grid into a curvilinear grid, a technique that is common to many grid generation schemes. Examples of this approach are given by **Caughey (1978)**, **Haussling (1979)**, and **Pope (1978)**.

The finite difference methods are more advantageous than the finite element methods which must be used on irregular grids. The fact is that finite differ-

ence methods can be used on irregular grids, as is evident from the works of **Frey (1977), Fritts and Boris (1979), Pavlin and Perrone (1979).** Furthermore, the co-ordinate transformation can be thought of as defining finite difference formulae for the corresponding curvilinear grid. The distinction between the two approaches is that an irregular grid need not be topologically regular, whereas the curvilinear grid corresponding to a co-ordinate transformation is always topologically regular (except at singular points of the transformation). Because it is not necessary that all interior points have the same number of neighbours, a fully irregular grid has greater flexibility for achieving variable resolution.

Too much irregularity can affect the accuracy of the computations for which the grid is intended. Consider the case of computations on a regular grid that involve variable coefficients. A co-ordinate transformation introduces variable coefficients into the transformed equations, so the variations of these coefficients must be well resolved by the regular grid in the transformed domain. In other words the transformation must be sufficiently smooth if computational difficulties are to be avoided. This constraint on the transformation is equivalent to a constraint on the corresponding curvilinear grid: the grid spacing must vary smoothly. And if spacing should vary smoothly for curvilinear grids, the same should be true for fully irregular grids.

Several techniques have been used to obtain smooth grids. These can be classified as the following:

(i) The simplest of these is to require that each interior grid point be at the position determined by the mean of the co-ordinates of its neighbours. The co-ordinates of all the points must be found simultaneously by solving a system of linear equations. It is necessary to know which points are neighbours before the equations can be formulated. This technique has been incorporated in the grid construction schemes of **Cavendish (1974)**, and **Yanenko et al. (1976).**

(ii) If the grid is constructed so that all interior points have the same number of neighbours, then this grid smoothing technique defines a co-ordinate transformation. **Amsden and Hirt (1973)** and **Barfield (1970)** have followed this approach to obtain smooth curvilinear grids. Again, the co-ordinates of all the points must be obtained simultaneously by solving a system of equations.

(iii) Another type of co-ordinate transformation that has been used to obtain smooth grids is prescribed by an interpolating function. This technique requires the construction of a regular grid which is transformed into an irregular grid within the computational domain. The positions of these special grid points are fixed by the user at the beginning of the construction process. Each element within the regular grid is subdivided into regularly shaped grid points which are then mapped into the computational domain. The interpolation function that maps these points is determined by the positions that have been specified for the fixed control points. **Hall et al. (1976)** use a bivariate blending function interpolation scheme developed by **Gordon and Hall (1973)**. **Zienkiewicz and Phillips (1971)** use the isoparametric interpolation schemes that are popularly used for finite element computations. **Cook (1974)** uses the linearly blended interpolation formulae of **Coons (1967)** in constructing grids for two-dimensional curved surfaces and for three-dimensional volumes.

(iv) A somewhat different approach to the problem of optimizing the grid is taken by **McNeice and Marcal (1971)**. Their grid is to be used to solve finite element equations based upon conditions of minimum energy. The value of the minimum energy depends on the grid configuration, so they vary the positions of the grid points to obtain a grid for which the minimum energy is least. Similarly **Babuska et al. (1975)** discuss grid optimization by local refinement during the course of the computations. **Cavendish (1975)** and **Cavendish et al. (1977)** point out that blending function interpolation is well suited for such local refinement.

Most of the work toward automating grid generation has dealt with two-dimen sional grids, either planar or curved. However, the more difficult three-dimensional problem has been discussed by **Cavendish et al. (1977)**, **Cook (1974)**, **Lau (1979)**, and **Zienkiewicz and Phillips (1971)**.

3.2. Computer Defined Surface Elements

A detailed mesh generation scheme is found unnecessary and time consuming for the present work. The hull surface about which the flow is to be computed is approximated by a large number of surface elements, whose characteristic dimensions are small compared to those of the main body. In fact this approach can be accepted as a rough mesh generation scheme. The surface elements are

simply obtained by the intersection between the hull surface and parallel planes. In general in order to represent a ship hull three mutually orthogonal views are constructed which are called sectional plans. The lines of each section do not completely specify a surface since if three dimensional data points are required, that lie between the lines, these must be obtained from some approximation procedure.

Polinomials have long been the functions most widely used to approximate other functions, mainly because they have the simplest mathematical properties. However, it is a common observation that a polynomial of moderately high degree fitted to a fairly large number of given data points tends to exhibit more numerous, and more severe undulations than a curve drawn with a spline. There is now considerable evidence that in many circumstances a spline function is a more adaptable approximating function than a polynomial involving a comparable number of parameters. This conclusion is based in part on actual numerical experience, and in part on mathematical demonstrations that the solutions of a variety of problems of *best* approximation actually turn out to be spline functions. In this work in order to create computer defined surface elements mathematical splines are used.

3.3. Spline Functions

In many industries, e.g., shipbuilding, automotive and aircraft, the final full or nearly full size shape is determined by a process called lofting. Early in the development of mathematical tools for computer aided geometric design there was considerable interest in developing a mathematical model of this process. As a result, the form of the mathematical spline is derived from its physical counterpart – the loftman's spline as shown in **(Figure 3-1)**. A physical spline is a long, narrow strip of wood or plastic used to fit curves through specified data points. The splines are shaped by lead weights called *ducks*. By varying the number and position of the lead weights the spline is made to pass through the specified data such that the resulting curve appears *smooth*, or *fair*, and *pleasing to the eye.*

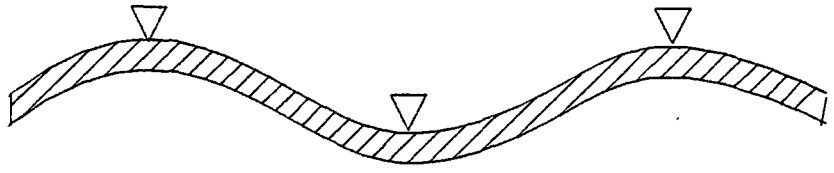

Figure 3-1. Physical spline and ducks.

Consider the physical spline as a thin elastic beam, the shape of the spline, corresponding to the deflection of the beam y, is obtained from Euler's equation for the bending moment $M(x)$ along the length of the beam. Specifically,

$$M(x) = \frac{EI}{R(x)}$$

where E is Young's modulus (determined by the material property of the beam), I is the moment of inertia (determined by the cross-sectional shape of the beam) and $R(x)$ is the radius of curvature of the beam.

For small deflections ($y' << 1$) the radius of curvature is approximated by

$$\frac{1}{R(x)} = \frac{y''}{(1+y'^2)^{3/2}} \simeq y''$$

where the prime denotes differentiation with respect to x, the distance along the beam, and y represents the deflection of the beam. Euler's equation then becomes

$$y'' = \frac{M(x)}{EI}$$

Assuming that the ducks act as simple supports, the bending moment $M(x)$ is known to vary linearly between supports. Substituting $M(x) = A(x) + B$, Euler's equation becomes

$$y'' = \frac{Ax + B}{EI}$$

Integrating twice yields

$$y = A_1 x^3 + B_1 x^2 + C_1 x + D_1$$

for the deflection of the beam. This result shows that the shape of the physical spline between ducks is mathematically described by cubic polynomials.

In general, the mathematical spline is a piecewise polynomial of degree K with continuity of derivatives of order $K-1$ at the common joints between segments. Thus, the cubic spline has second-order or C^2 continuity at the joints. Piecewise splines of low-degree polynomials are most useful for curve fitting because low-degree polynomials both reduce the computational requirements and also reduce numerical instabilities that arise with higher degree curves. These instabilities cause undesirable oscillations when several points are joint in a common curve. However, since low-degree polynomials can not span an arbitrary series of points, adjacent polynomial segments are used. Based on these considerations and the analogy with the physical spline, a common technique is to use a series of cubic spline segments with each segment spanning only two points. Further, the cubic spline is advantageous since it is the lowest degree curve which allows a point of inflection and which has the ability to twist through space.

The equation for a single parametric cubic spline segment is given by

$$P(t) = \sum_{i=1}^{4} B_i t^{i-1} \qquad t_1 \le t \le t_2 \tag{3.1}$$

where t_1 and t_2 are the parameter values at the beginning and end of the segment. $P(t)$ is the position vector of any point on the cubic spline segment. $P(t) = [x(t) \quad y(t) \quad z(t)]$ is a vector valued function. The three components of $P(t)$ are the Cartesian co-ordinates of the position vector. Each component has a similar formulation to $P(t)$, i.e.,

$$x(t) = \sum_{i=1}^{4} B_{i_x} t^{i-1} \qquad t_1 \le t \le t_2$$

$$y(t) = \sum_{i=1}^{4} B_{i_y} t^{i-1} \qquad t_1 \le t \le t_2$$

$$z(t) = \sum_{i=1}^{4} B_{i_z} t^{i-1} \qquad t_1 \le t \le t_2$$

The constant coeficients B_i are determined by specifying four boundary conditions for the spline segment. Writing out Eq.(3.1) yields

$$P(t) = B_1 + B_2 t + B_3 t^2 + B_4 t^3 \qquad t_1 \le t \le t_2 \tag{3.2}$$

Let P_1 and P_2 be the position vectors at the ends of the spline segment as shown in **Figure 3-2.** Also let P_1' and P_2', the derivatives with respect to t, be

the tangent vectors at the ends of the spline segment. Differentiating Eq.(3.1) yields

$$P'(t) = [x'(t) \quad y'(t) \quad z'(t)] = \sum_{i=1}^{4} B_i(i-1)t^{i-2} \qquad t_1 \le t \le t_2 \tag{3.3}$$

Writing this result out gives

$$P'(t) = B_2 + 2B_3t + 3B_4t^2 \qquad t_1 \le t \le t_2 \tag{3.4}$$

Assuming, without loss of generality, that $t_1 = 0$, and applying the four boundary conditions,

$$P(0) = P_1 \tag{3.5a}$$

$$P(t_2) = P_2 \tag{3.5b}$$

$$P'(0) = P_1' \tag{3.5c}$$

$$P'(t_2) = P_2' \tag{3.5d}$$

yields four equations for the unknown B_i's. Specifically,

$$P(0) = B_1 = P_1 \tag{3.6a}$$

$$P'(0) = \sum_{i=1}^{4} (i-1)t^{i-2}B_i|_{t=0} = B_2 = P_1' \tag{3.6b}$$

$$P(t_2) = \sum_{i=1}^{4} B_i t^{i-1}|_{t=t_2} = B_1 + B_2t_2 + B_3{t_2}^2 + B_4{t_2}^3 \tag{3.6c}$$

$$P'(t_2) = \sum_{i=1}^{4} (i-1)t^{i-2}B_i|_{t=t_2} = B_2 + 2B_3t_2 + 3B_4{t_2}^2 \tag{3.6d}$$

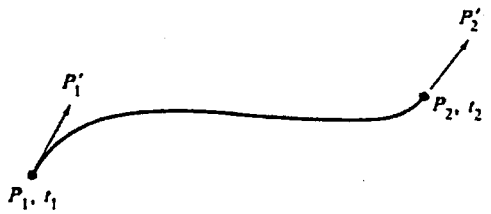

Figure 3-2. Single cubic spline segment

Solving for B_3 and B_4 yields

$$B_3 = \frac{3(P_2 - P_1)}{{t_2}^2} - \frac{2P_1'}{t_2} - \frac{P_2'}{t_2} \tag{3.7a}$$

and

$$B_4 = \frac{2(P_1 - P_2)}{{t_2}^3} + \frac{P_1'}{{t_2}^2} + \frac{P_2'}{{t_2}^2} \qquad \textbf{(3.7b)}$$

These values of B_1,B_2,B_3 and B_4 determine the cubic spline segment. Note that the shape of the segment depends on the position and tangent vectors at the ends of the segment. Further, notice that the value of the parameter $t = t_2$ at the end of the segment occurs in the results. Since each of the end position and tangent vectors has three components, the parametric equation for a cubic space curve depends on twelve vector components and the parameter value t_2 at the end of the segment.

Substituting Eqs.(3.6) and (3.7) into Eq.(3.1) yields the equation for a single cubic spline segment:

$$\begin{aligned} P(t) = P_1 + P_1' t + \left[\frac{3(P_2 - P_1)}{{t_2}^2} - \frac{2P_1'}{t_2} - \frac{P_2'}{t_2}\right] t^2 \\ + \left[\frac{2(P_1 - P_2)}{{t_2}^3} + \frac{P_1'}{{t_2}^2} + \frac{P_2'}{{t_2}^2}\right] t^3 \end{aligned} \qquad \textbf{(3.8)}$$

Equation (5.8) is for a single cubic spline segment. However, to represent a complete curve, multiple segments are joined together. Two adjacent segments are shown in **Figure 3-3**. Provided that the position vectors P_1, P_2, P_3, the tangent vectors P_1', P_2', P_3' and the parameter values t_2, t_3 are known, then Eq.(5.8), applied to each of the two segments, yields their shapes. However, it is unlikely that tangent vector P_2' at the internal joint between the two segmants is known. Fortunately, the internal tangent vector P_2' can be determined by imposing a continuity condition at the internal joint.

Recall that a piecewise spline of degree K has continuity of order $K - 1$ at the internal joints. Thus, a cubic spline has second-order continuity at the internal joints. This means that the second derivative $P_2''(t)$ is continuous across the joint; i.e., the curvature is continuous across the joint. Differentiating Eq.(3.1) twice yields

$$P''(t) = \sum_{i=1}^{4} (i-1)(i-2) B_i t^{i-3} \qquad t_1 \le t \le t_2 \qquad \textbf{(3.9)}$$

Noting that for the first cubic spline segment the parameter range is $0 \le t \le t_2$, evaluating Eq.(3.9) at the end of the segment where $t = t_2$ gives

$$P'' = 6B_4 t_2 + 2B_3$$

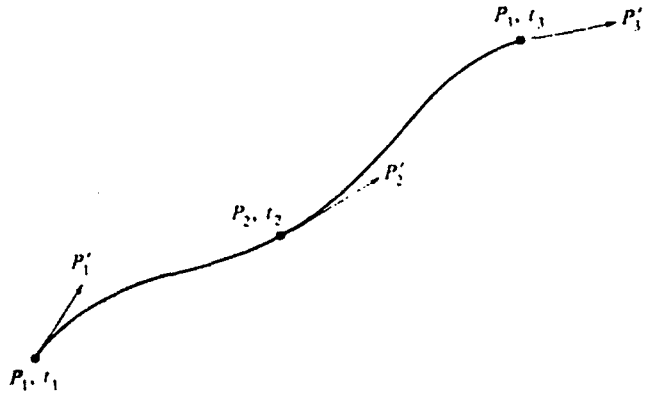

Figure 3-3. Two piecewise cubic spline segments.

For the second cubic spline segment the parameter range is $0 \leq t \leq t_3$. Evaluating Eq.(3.9) at the beginning of this second segment where $t = 0$ yields

$$P'' = 2B_3$$

Equating these two results and using Eqs.(3-6a,b) and (3-7a) yields

$$6t_2\left[\frac{2(P_1 - P_2)}{{t_2}^3} + \frac{P_1'}{{t_2}^2} + \frac{P_2'}{{t_2}^2}\right] + 2\left[\frac{3(P_2 - P_1)}{{t_2}^2} - \frac{2P_1'}{t_2} - \frac{P_2'}{t_2}\right]$$
$$= 2\left[\frac{3(P_3 - P_2)}{{t_3}^2} - \frac{2P_2'}{t_3} - \frac{P_3'}{t_3}\right]$$

Here the left hand side of the equation represents the curvature at the end of the first segment and the right hand side the curvature at the beginning of the second segment. Multiplying by $t_2 t_3$ and collecting the terms gives

$$t_3 P_1' + 2(t_3 + t_2)P_2' + t_2 P_3' = \frac{3}{t_2 t_3}\left[{t_2}^2(P_3 - P_2) + {t_3}^2(P_2 - P_1)\right] \qquad \textbf{(3.10)}$$

which can be solved for P_2', the unknown tangent vector at the internal joint.

These results can be generalized for n data points to give $n - 1$ piecewise cubic spline segments with position, slope, and curvature. Using the notation shown in **Figure 3-4** the generalized equations for any two adjacent cubic spline segment $P_k(t)$ and $P_{k+1}(t)$ are:

$$P_k(t) = P_k + P'_k t + \left[\frac{3(P_{k+1} - P_k)}{{t_{k+1}}^2} - \frac{2P'_k}{t_{k+1}} - \frac{P'_{k+1}}{t_{k+1}}\right] t^2 + \left[\frac{2(P_k - P_{k+1})}{{t_{k+1}}^3} + \frac{P'_k}{{t_{k+1}}^2} + \frac{P'_{k+1}}{{t_{k+1}}^2}\right] t^3 \tag{3.11}$$

for the first segment, and

$$P_{k+1}(t) = P_{k+1} + P'_{k+1} t + \left[\frac{3(P_{k+2} - P_{k+1})}{{t_{k+2}}^2} - \frac{2P'_{k+1}}{t_{k+2}} - \frac{P'_{k+2}}{t_{k+2}}\right] t^2 + \left[\frac{2(P_{k+1} - P_{k+2})}{{t_{k+2}}^3} + \frac{P'_{k+1}}{{t_{k+2}}^2} + \frac{P'_{k+2}}{{t_{k+2}}^2}\right] t^3 \tag{3.12}$$

for the second segment.Recalling that the parameter range begins at zero for each segment, for the first segment $0 \leq t \leq t_{k+1}$ and for the second $0 \leq t \leq t_{k+2}$.

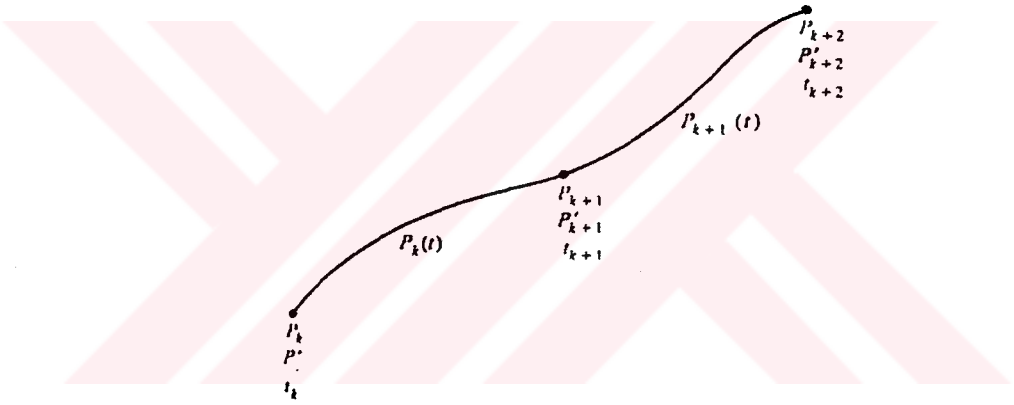

Figure 3-4. Notation for multiple piecewise cubic spline segments.

For any two adjacent spline segments, equating the second derivatives at the common internal joint, i.e., letting $P''_k(t_k) = P''_{k+1}(0)$, yields the generalized result, equivalent to Eq.(3.10), i.e.,

$$t_{k+2}P'_k + 2(t_{k+1} + t_{k+2})P'_{k+1} + t_{k+1}P'_{k+2} = \frac{3}{t_{k+1}t_{k+2}}\left[{t_{k+1}}^2(P_{k+2} - P_{k+1}) + {t_{k+2}}^2(P_{k+1} - P_k)\right] \quad 1 \leq k \leq n-2 \tag{3.13}$$

for determining the tangent vector at the internal joint between any two spline segments P_k and P_{k+1}.

Applying Eq.(3.13) recursively over all the spline segments yields $n-2$ equations for the tangent vectors P'_k, $2 \leq k \leq n-1$. In matrix form the result is

$$\begin{pmatrix} t_3 & 2(t_2+t_3) & 0 & \dots & \dots & \dots & \dots & \dots \\ 0 & t_4 & 2(t_3+t_4) & t_3 & 0 & \dots & \dots & \dots \\ 0 & 0 & t_5 & 2(t_4+t_5) & t_4 & 0 & \dots & \dots \\ \vdots & \vdots & \vdots & \vdots & \dots & \dots & \dots & \dots \\ \dots & \dots & \dots & \dots & 0 & t_n & 2(t_n+t_{n-1}) & t_{n-1} \end{pmatrix} \times \begin{pmatrix} P_1' \\ P_2' \\ P_3' \\ \vdots \\ P_n' \end{pmatrix}$$

$$= \begin{pmatrix} \frac{3}{t_2 t_3}\{{t_2}^2(P_3-P_2)+{t_3}^2(P_2-P_1)\} \\ \frac{3}{t_3 t_4}\{{t_3}^2(P_4-P_3)+{t_4}^2(P_3-P_2)\} \\ \vdots \\ \frac{3}{t_{n-1} t_n}\{{t_{n-1}}^2(P_n-P_{n-1})+{t_n}^2(P_{n-1}-P_{n-2})\} \end{pmatrix} \qquad \textbf{(3.14)}$$

or

$$[M^*][P'] = [R]$$

Since there are only $n-2$ equations for the n tangent vectors, $[M^*]$ is not square and thus cannot be inverted to obtain the solution for $[P']$; i.e., the problem is indeterminate. But assuming that the tangent vectors P_1' and P_n' are known, the problem becomes determinate. The matrix formulation is now

$$\begin{pmatrix} 1 & 0 & \dots & \dots & \dots & \dots & \dots & \dots \\ t_3 & 2(t_2+t_3) & 0 & \dots & \dots & \dots & \dots & \dots \\ 0 & t_4 & 2(t_3+t_4) & t_3 & 0 & \dots & \dots & \dots \\ 0 & 0 & t_5 & 2(t_4+t_5) & t_4 & 0 & \dots & \dots \\ \vdots & \vdots & \vdots & \vdots & \dots & \dots & \dots & \dots \\ \dots & \dots & \dots & \dots & 0 & t_n & 2(t_n+t_{n-1}) & t_{n-1} \\ \dots & \dots & \dots & \dots & \dots & \dots & 0 & 1 \end{pmatrix} \times \begin{pmatrix} P_1' \\ P_2' \\ P_3' \\ \vdots \\ \vdots \\ P_n' \end{pmatrix}$$

$$= \begin{pmatrix} P_1' \\ \frac{3}{t_2 t_3}\{{t_2}^2(P_3-P_2)+{t_3}^2(P_2-P_1)\} \\ \frac{3}{t_3 t_4}\{{t_3}^2(P_4-P_3)+{t_4}^2(P_3-P_2)\} \\ \vdots \\ \frac{3}{t_{n-1} t_n}\{{t_{n-1}}^2(P_n-P_{n-1})+{t_n}^2(P_{n-1}-P_{n-2})\} \\ P_n' \end{pmatrix} \qquad \textbf{(3.15)}$$

or

$$[M][P'] = [R]$$

where $[M]$ is now square and invertible. Notice also that $[M]$ is tridiagonal†, which reduces the computational work required to invert it. Further, $[M]$ is

† A tridiagonal matrix is one in which coefficients appear only on the main, first upper and first lower diagonals.

diagonally dominant †. Hence it is nonsingular, and inversion yields a unique solution. The solution for $[P']$ is thus

$$[P'] = [M]^{-1}[R] \tag{3.16}$$

Once the P'_k's are known, the B_i coefficients for each spline segment can be determined. Generalizing Eqs.(3.6)-(3.11) yields

$$\begin{aligned} B_{1k} &= P_k \\ B_{2k} &= P'_k \\ B_{3k} &= \frac{3(P_{k+1} - P_k)}{{t_{k+1}}^2} - \frac{2P'_k}{t_{k+1}} - \frac{P'_{k+1}}{t_{k+1}} \\ B_{4k} &= \frac{2(P_k - P_{k+1})}{{t_{k+1}}^3} + \frac{P'_k}{{t_{k+1}}^2} + \frac{P'_{k+1}}{{t_{k+1}}^2} \end{aligned}$$

Recalling that the P_k's and P'_k's are vector valued confirms that the B_i's are also vector valued; i.e., if the P_k's and P'_k's have x, y, z components then theB_i's also have x, y, z components.

In matrix form these equations for any spline segment k are

$$\begin{aligned} [B] &= \begin{pmatrix} B_{1k} \\ B_{2k} \\ B_{3k} \\ B_{4k} \end{pmatrix} \\ &= \begin{pmatrix} 1 & 0 & 0 & 0 \\ 0 & 1 & 0 & 0 \\ \frac{-3}{{t_{k+1}}^2} & \frac{-2}{t_{k+1}} & \frac{3}{{t_{k+1}}^2} & \frac{-1}{t_{k+1}} \\ \frac{2}{{t_{k+1}}^3} & \frac{1}{{t_{k+1}}^2} & \frac{-2}{{t_{k+1}}^3} & \frac{1}{{t_{k+1}}^2} \end{pmatrix} \times \begin{pmatrix} P_k \\ P'_k \\ P_{k+1} \\ P'_{k+1} \end{pmatrix} \end{aligned} \tag{3.17}$$

To generate a piecewise cubic spline through n given position vectors P_k, $1 \leq k \leq n$, with end tangent vectors P'_1 and P'_n, Eq.(3.16) is used to determine the integral tangent vectors P'_k, $2 \leq k \leq n-1$. Then for each piecewise cubic spline segment the end position and tangent vectors for that segment are used to determine the B_{ik}'s, $1 \leq i \leq 4$ for that segment using Eq.(3.17). Finally the generalization of Eq.(3.1)

$$P_k(t) = \sum_{i=1}^{4} B_{ik} t^{i-1} \qquad 0 \leq t \leq t_{k+1}, \quad 1 \leq k \leq n-1 \tag{3.18}$$

† In a tridiagonally dominant matrix the magnitude of the terms on the main diagonal exceed that of the off-diagonal terms on the same row.

is used to determine points on the spline segment.

In matrix form Eq.(3.18) becomes

$$P_k(t) = [1 \quad t \quad t^2 \quad t^3] \times \begin{pmatrix} B_{1k} \\ B_{2k} \\ B_{3k} \\ B_{4k} \end{pmatrix} \qquad 0 \leq t \leq t_{k+1} \tag{3.19}$$

Substituting Eq.(3.17) and rearranging yields

$$P_k(\tau) = [F_1(\tau) \quad F_2(\tau) \quad F_3(\tau) \quad F_4(\tau)] \times \begin{pmatrix} P_k \\ P'_k \\ P_{k+1} \\ P'_{k+1} \end{pmatrix} \quad \begin{cases} 0 \leq \tau \leq 1 \\ 1 \leq k \leq n-1 \end{cases} \tag{3.20}$$

where

$$\tau = (t/t_{k+1})$$

$$F_{1k}(\tau) = 2\tau^3 - 3\tau^2 + 1 \tag{3.21a}$$

$$F_{2k}(\tau) = -2\tau^3 + 3\tau^2 \tag{3.21b}$$

$$F_{3k}(\tau) = \tau(\tau^2 - 2\tau + 1)t_{k+1} \tag{3.21c}$$

$$F_{4k}(\tau) = \tau(\tau^2 - \tau)t_{k+1} \tag{3.21d}$$

are called blending or weighting functions.

Using the definition of the blending functions Eq.(3.20) is written in matrix form as

$$P_k(\tau) = [F][G] \tag{3.22}$$

where $[F]$ is a blending function matrix given by

$$[F] = [F_1(\tau) \quad F_2(\tau) \quad F_3(\tau) \quad F_4(\tau)] \tag{3.23}$$

and

$$[G]^T = [P_k \quad P_{k+1} \quad P'_k \quad P'_{k+1}] \tag{3.24}$$

contains the geometric information. Equations of the form of Eqs.(3.22), i.e., a matrix of blending functions times a matrix of geometric conditions, frequently appear in curve and surface descriptions.

In general the end position vectors have relatively more influence than the end tangent vectors. Recall that a piecewise cubic spline curve is determined by the

position vectors, tangent vectors and the parameter values, i.e., the t_k's at the end of each segment. The choice of the t_k's affects the curve smoothness.

Continuity of the second derivatives at the internal joints does not in itself produce a fair or smooth cubic spline curve in the sense of minimum curvature along the curve. To obtain minimum curvature and hence maximium smoothness, the coefficients B_3 and B_4 must be minimized for each segment by choosing appropriate values for the t_k's for each segment. This additional computational effort is normally not required.

One approach used to determine the t_k's is to normalize the variation by choosing $t_k = 1.0$ for each cubic segment. This choice simplifies the computational requirements (see **Section 3.4**). As can be seen from the previous equations, each choice of t_k produces different coefficient values and, hence, different curves through the given data points.

3.4. Normalized Cubic Splines

An alternate approximation for the t_k spline segment parameter values is to normalize them to unity. Thus, $0 \leq t \leq 1$ for all segments.

The blending functions†, now become

$$F_1(t) = 2t^3 - 3t^2 + 1 \tag{3.25a}$$

$$F_2(t) = -2t^3 + 3t^2 \tag{3.25b}$$

$$F_3(t) = t^3 - 2t^2 + t \tag{3.25c}$$

$$F_4(t) = t^3 - t^2 \tag{3.25d}$$

For the normalized cubic spline the blending function matrix is now written as

$$[F] = [T][N] = [t^3 \quad t^2 \quad t \quad 1] \times \begin{pmatrix} 2 & -2 & 1 & 1 \\ -3 & 3 & -2 & -1 \\ 0 & 0 & 1 & 0 \\ 1 & 0 & 0 & 0 \end{pmatrix} \tag{3.26}$$

† These blending functions are the cubic Hermite polynomial blending functions on the interval $0 \leq t \leq 1$.

The matrix equation for a cubic spline segment, Eq.(3.22), can now be written as

$$P(t) = [F][G] = [T][N][G] \tag{3.27}$$

Notice that $[T]$ and $[N]$ are constant for all cubic spline segments. Only the geometry matrix $[G]$ changes from segment to segment.

Equation (3.15), used to determine the interval tangent vectors required in $[G]$, now becomes

$$\begin{pmatrix} 1 & 0 & \dots & \dots & \dots & \dots \\ 1 & 4 & 1 & 0 & \dots & \dots \\ 0 & 1 & 4 & 1 & 0 & \dots \\ \dots & \dots & \dots & \dots & \dots & \dots \\ \dots & \dots & 0 & 1 & 4 & 1 \\ \dots & \dots & \dots & \dots & 0 & 1 \end{pmatrix} \times \begin{pmatrix} P'_1 \\ P'_2 \\ P'_3 \\ \vdots \\ \vdots \\ P'_n \end{pmatrix} = \begin{pmatrix} 3\{(P_3 - P_2) + (P_2 - P_1)\} \\ 3\{(P_4 - P_3) + (P_3 - P_2)\} \\ \vdots \\ 3\{(P_n - P_{n-1}) + (P_{n-1} - P_{n-2})\} \end{pmatrix} \tag{3.28}$$

The solution is again given by Eq.(3.16). However, here $[M]$ is constant and need only be inverted once. When the number of position vectors is large, this represents a considerable savings in computational expense.

One final point is of interest. If, for the normalized spline, the matrix $[B]^T = [B_1 \quad B_2 \quad B_3 \quad B_4]$ is known, then the geometry matrix for the spline segment, i.e., $[G]$, is given by

$$[G] = [N]^{-1}[B]^T$$

where $[N]^{-1}$, the inverse of $[N]$, is

$$[N]^{-1} = \begin{pmatrix} 0 & 0 & 0 & 1 \\ 1 & 1 & 1 & 1 \\ 0 & 0 & 1 & 1 \\ 3 & 2 & 1 & 0 \end{pmatrix} \tag{3.29}$$

Points along the spline segment are again obtained using Eq.(3.27).

CHAPTER 4. NUMERICAL RESULTS

Preparation of input data for the programme DAWSON.FOR needs a large amount of manual work. A large portion of the time devoted to this work is spent, mostly on distributing panels on the hull surface as well as on a portion of the free surface. Input data consists of two sets of data: the first one gives the co-ordinates of the vertices of the quadrilateral elements which we call *panels* and the second one contains integer values asigned to these vertices which we call *indices.*

4.1. Description of the Programmes

To reduce the manual work, two computer programmes are developed: one generating hull surface data and the other generating free surface data. The user of these programmes is free to dense the panel distributions. Two AutoCAD plotting routines are appended to these programmes. These routines enable the user to visualize and check if the panels are distributed properly. In case of peculiar panel distribution the user is free to go back and change the positions of waterlines and transverse sections which intersect to give out quadrilateral panels.

4.1.a. Programme APGOSH.FOR

This programme generates panels over a given ship hull. Using the offsets as input data it defines the hull surface by spline functions. Hence, gives the location of vertices of quadrilateral panels which were generated by the intersection of waterlines and transverse sections. The co-ordinates of vertices are given according to the global co-ordinate axis which are fixed on the ship hull as can be seen from **Figure 4-1.** Vertices are automatically numbered. The numbers, each of which resembles a vertex of a quadrilateral are given in the order which designates the normal vector pointed to the water. Hence, the numbers for the hull surface panels are given in clock-wise order when viewed from outside as shown in **Figure 4-2a.**

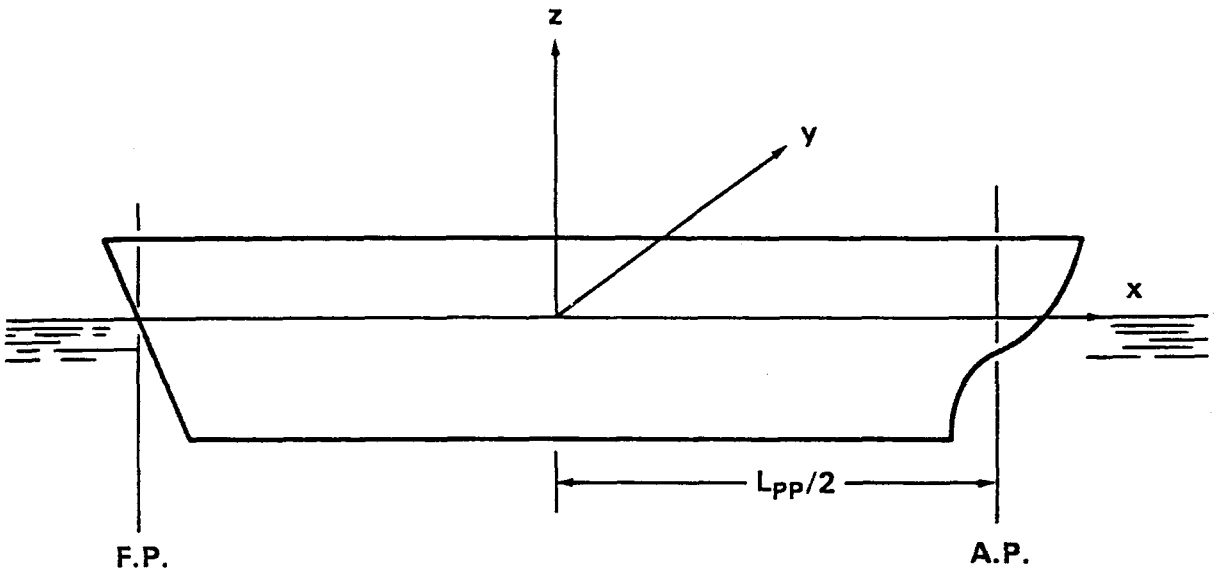

Figure 4-1. Global co-ordinate axis.

4.1.b. Programme APGOFS.FOR

This programme generates streamlines around a given ship hull. Then gives the location of vertices of quadrilateral panels placed between the streamlines and the the vertical lines which were determined by the user as an input. The co-ordinates of the vertices are given according to the global co-ordinate axis which are fixed on the ship hull. The vertices are automatically numbered by the programme and they follow one after another along every streamline beginning from upstream towards downstream. The numbers each of which resembles a vertex of a quadrilateral are given in the order which designates the normal vector pointed to the water. Hence, the numbers for the free surface panels are given in counter-clock-wise order when viewed from above the free surface as shown in **Figure 4-2b**. The panels on the free surface follow one after another along every streamline as the vertices do. But the first column of panels on the upstream edge of each streamline are given at the end of the related data in the order: closest panel to ship first, farthest panel last.

The field points distributed all over the region considered as if they were located at the middle of the probable streamlines. First row of the field points are chosen to be placed at the middle of each panel generated between the first streamline

and the hull contour.

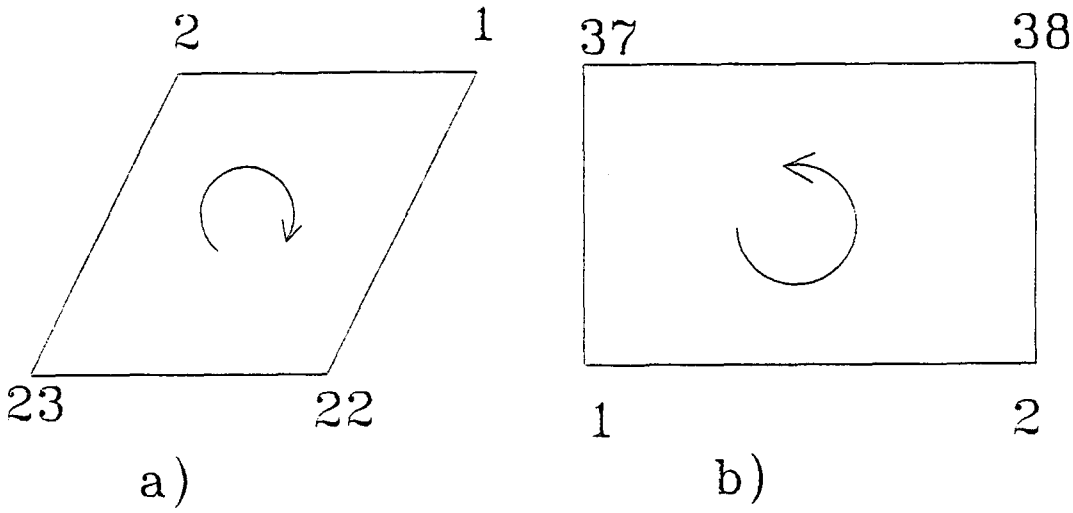

Figure 4-2. Order of panel numbers given a)on the ship hull surface, b)on the free surface.

4.2. Panel Arrangements

In this section the effect of the increase in the number of panels both on the ship hull surface and on the free surface is examined. **Dawson (1979)** reported that numerical experiments have convinced him that it is necessary to extend the local region of the free surface about 3/8 of a ship length to the side and represent the local region at least with eight rows of panels and it is necessary to take smaller panels near the bow and stern and also near the hull-free surface intersection than elsewhere.

Previous experience gives us the hint that as the number of panels is increased more accurate results are obtained.

As the number of panels is increased both the free surface and the ship hull surface are defined better, but more computing time is required. Once the panels are generated and the input data is prepared by the pre-processor programmes, using an Apollo HP with 16MB REM shortens the computing time. Two separate AutoCAD routines are appended to each of the preprocessor programmes which enable the user to visualize the panel arrangements and check if the panels are distributed properly. It was impossible to use an Apollo HP with these AutoCAD routines. Hence a PC with 8MB REM is used to generate input data. It was advantageous to work with the PC upto a total number of 515

panels. With the PC one can visualize the panel arrangements but one can not use more than 515 panels. After a total of 515 panels is reached the memory of the PC exhausts.

It was more important for the author to visualize the panels than to use more than 515 panels at the stage of developing the pre-processor programmes. Hence, it was decided to use the PC and care is taken in preparing the input data with restricted number of panels for the programme DAWSON.FOR.

The panel arrangements on the ship hull surface and on the free surface are made with the above suggestions and constraints in mind.

4.2.a. Wigley's Parabolic Hull

Four different panel arrangements are made for the Wigley's parabolic hull. These different panel arrangements both on the free surface and on the ship hull surface are shown in **Figures 4-3a** through **4-3d** and in **Figures 4-4a** through **4-4d**, respectively.

i) In the first panel arrangement 10 equally distributed panels along the ship hull surface are used. 16 panels are taken along the longitudinal direction on the free surface. A total of 144 panels on the free surface and 50 panels on the ship hull surface are used.

ii) In the second panel arrangement, near the bow and stern regions smaller panels are used. 14 panels are used along the ship hull surface and 25 panels are distributed along the longitudinal direction on the free surface. A total of 234 panels on the free surface and 70 panels on the ship hull surface are considered.

iii) In the third panel arrangement, equally distributed panels along the ship hull surface are considered again as in the first panel arrangement, but 20 panels instead of 10 are used. 32 panels are taken along the longitudinal direction on the free surface. A total of 288 panels on the free surface and 100 panels on the ship hull surface are used.

iv) In the fourth panel arrangement, near the bow and stern regions smaller

panels are taken. 26 panels are distributed along the ship hull surface and 42 panels are distributed along the longitudinal direction on the free surface. A total of 378 panels on the free surface and 130 panels on the ship hull surface are used.

At a total number of 508 panels (378 panels on the free surface, 130 panels on the hull surface) fairly good results are obtained.

4.2.b. Series-60 Hull

Some panel arrangements like the ones used for Wigley's parabolic hull are tried. One panel arrangement with sufficient number of panels for the Series-60 hull is given in **Figures 4-5a** and **4-5b.**

Along the ship hull surface 20 panels are used. These panels are not equally distributed. Near the bow and stern regions smaller panels are taken. 33 panels are distributed along the longitudinal direction on the free surface. A total of 297 panels on the free surface and 200 panels on the ship hull surface are used.

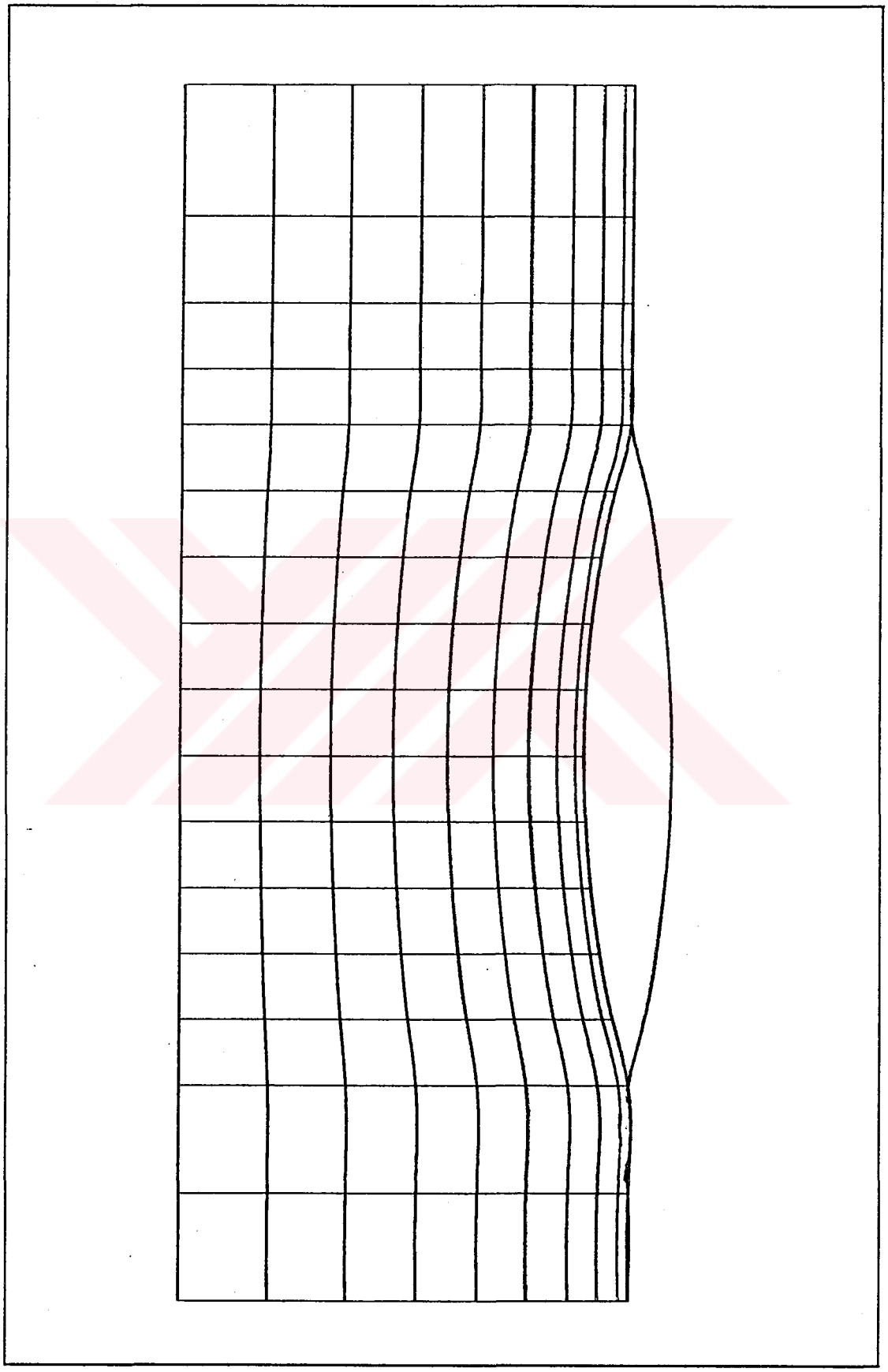

Figure 4-3a. Wigley hull first panel arrangement on the free surface.

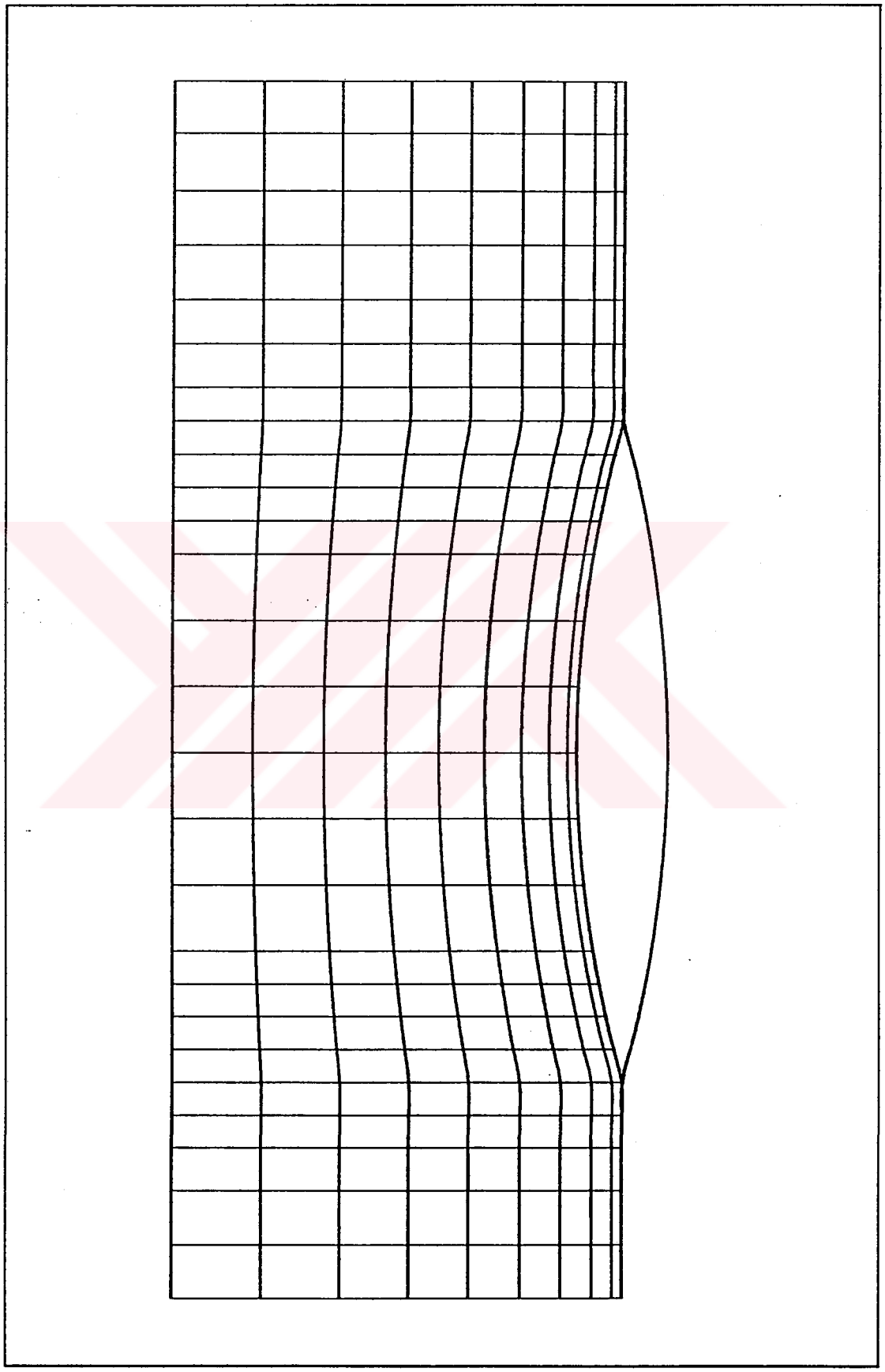

Figure 4-3b. Wigley hull second panel arrangement on the free surface.

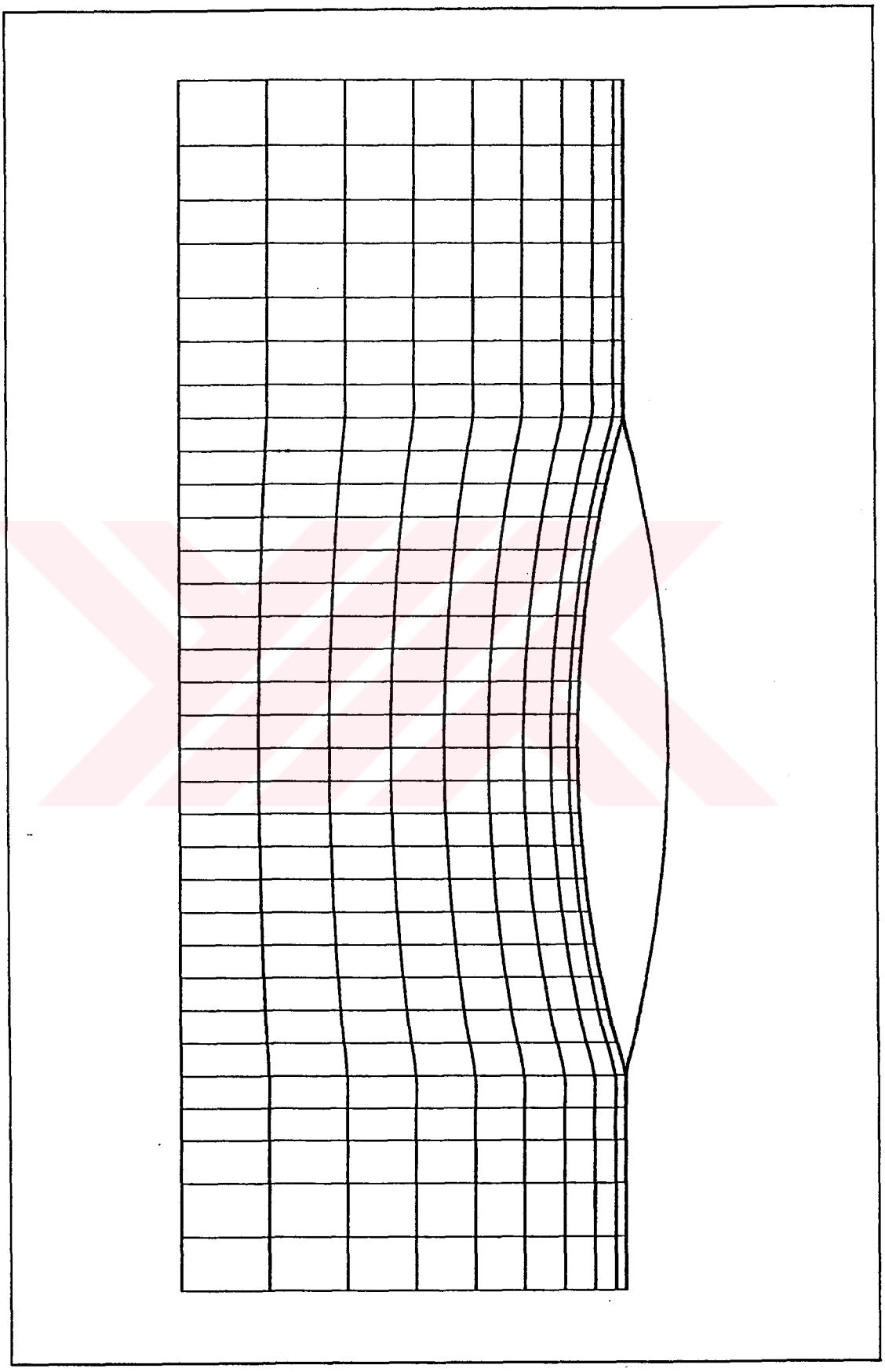

Figure 4-3c. Wigley hull third panel arrangement on the free surface.

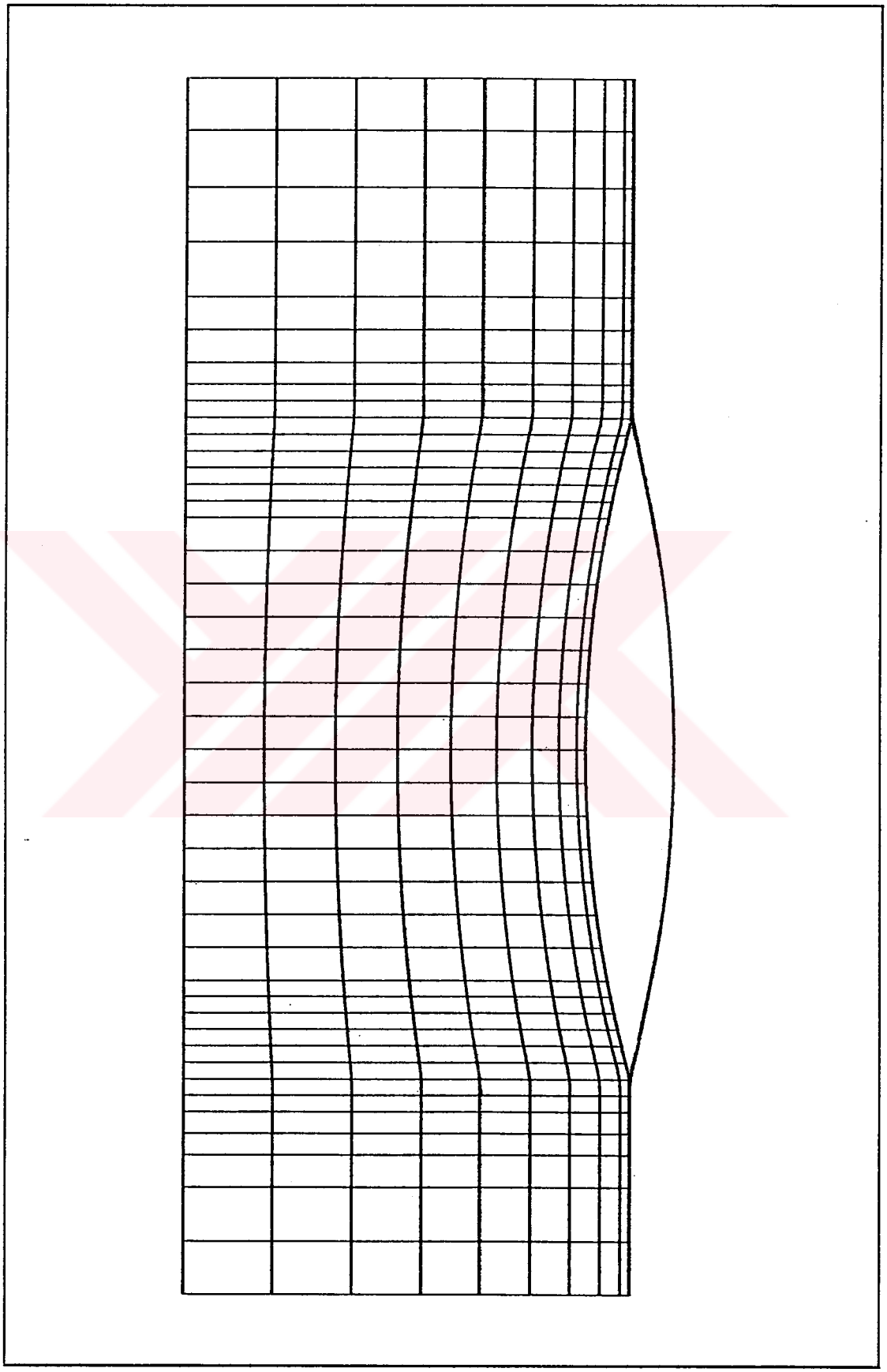

Figure 4-3d. Wigley hull fourth panel arrangement on the free surface.

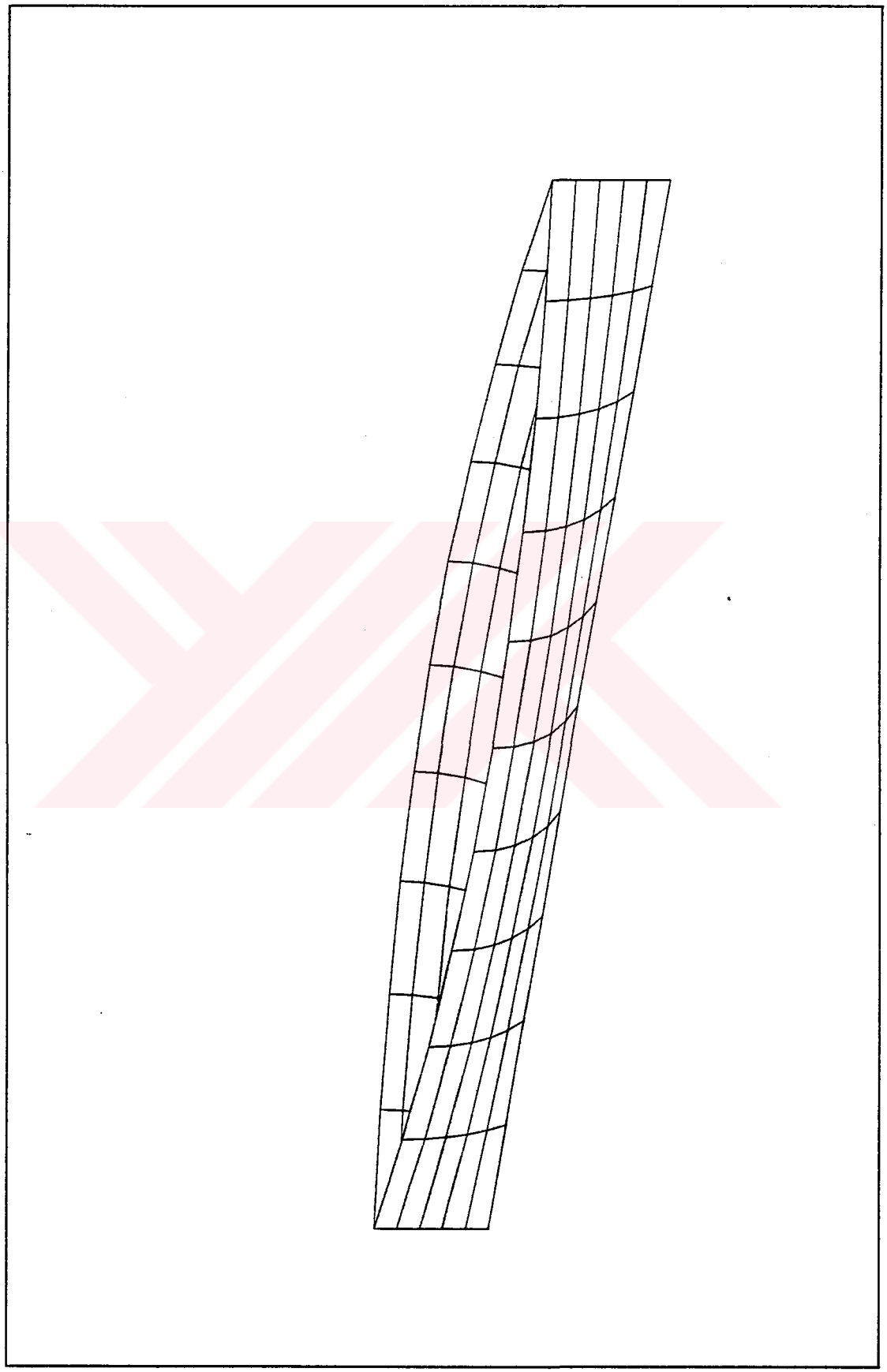

Figure 4-4a. Wigley hull first panel arrangement on the ship hull surface.

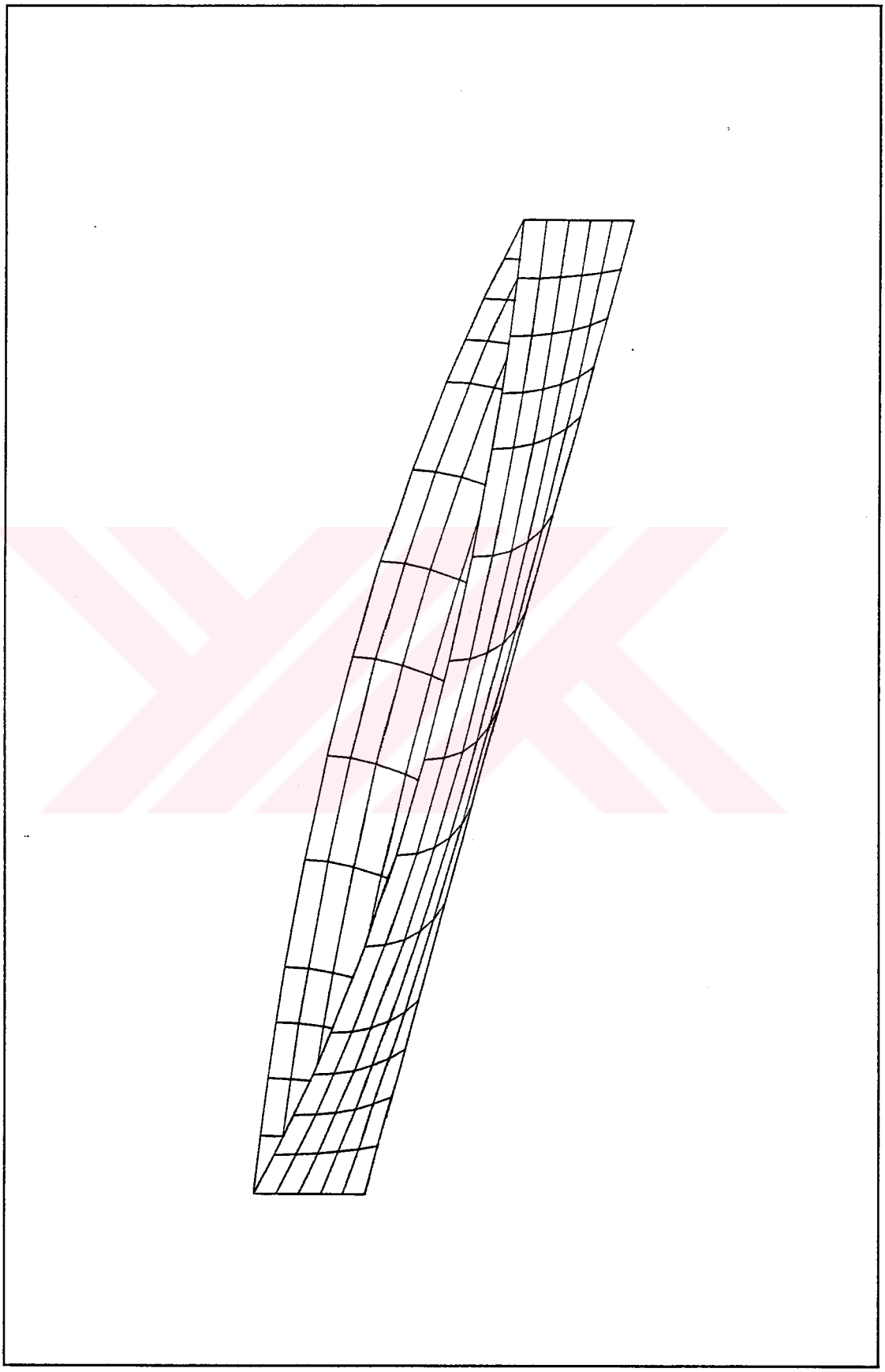

Figure 4-4b. Wigley hull second panel arrangement on the ship hull surface.

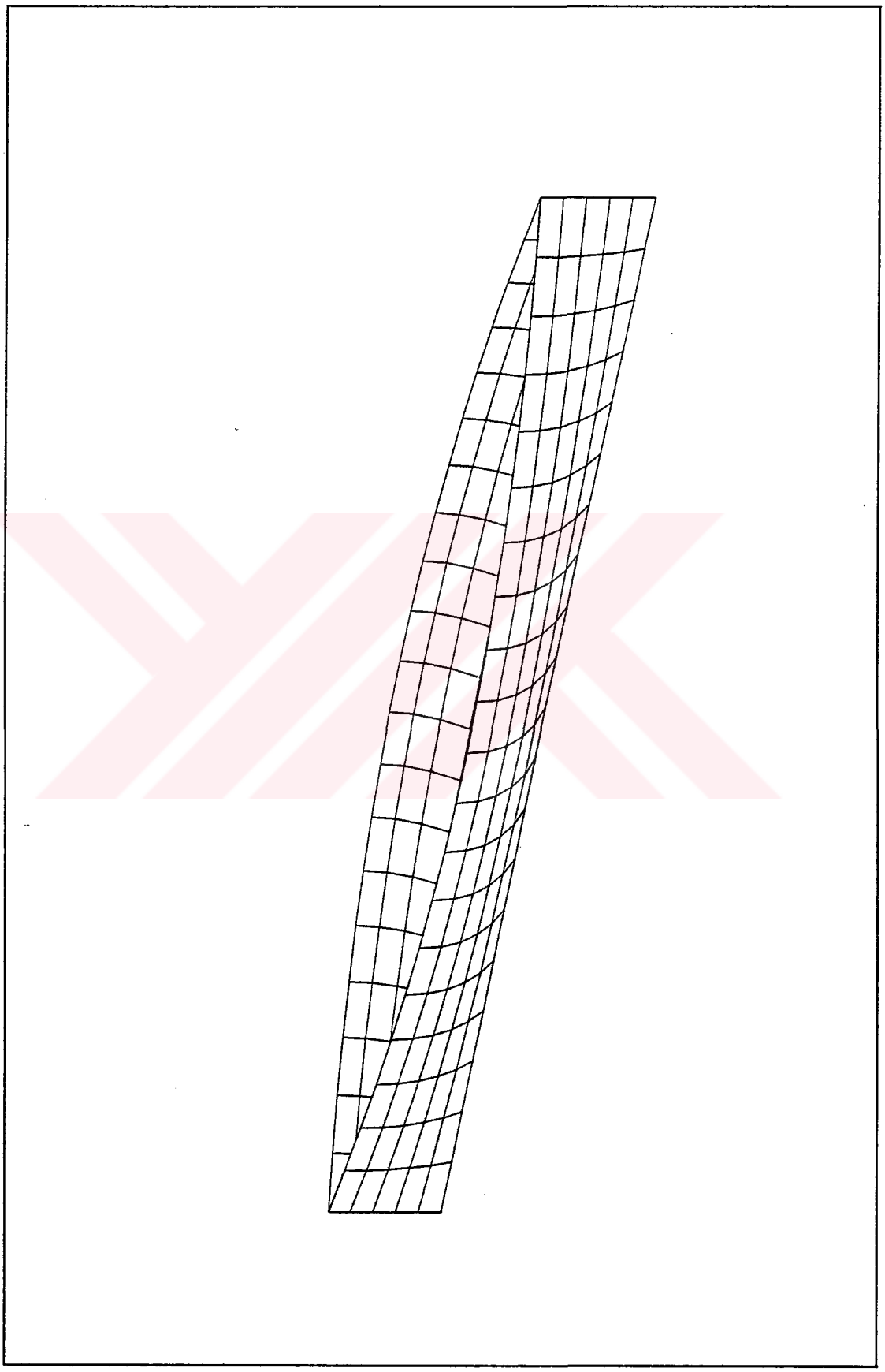

Figure 4-4c. Wigley hull third panel arrangement on the ship hull surface.

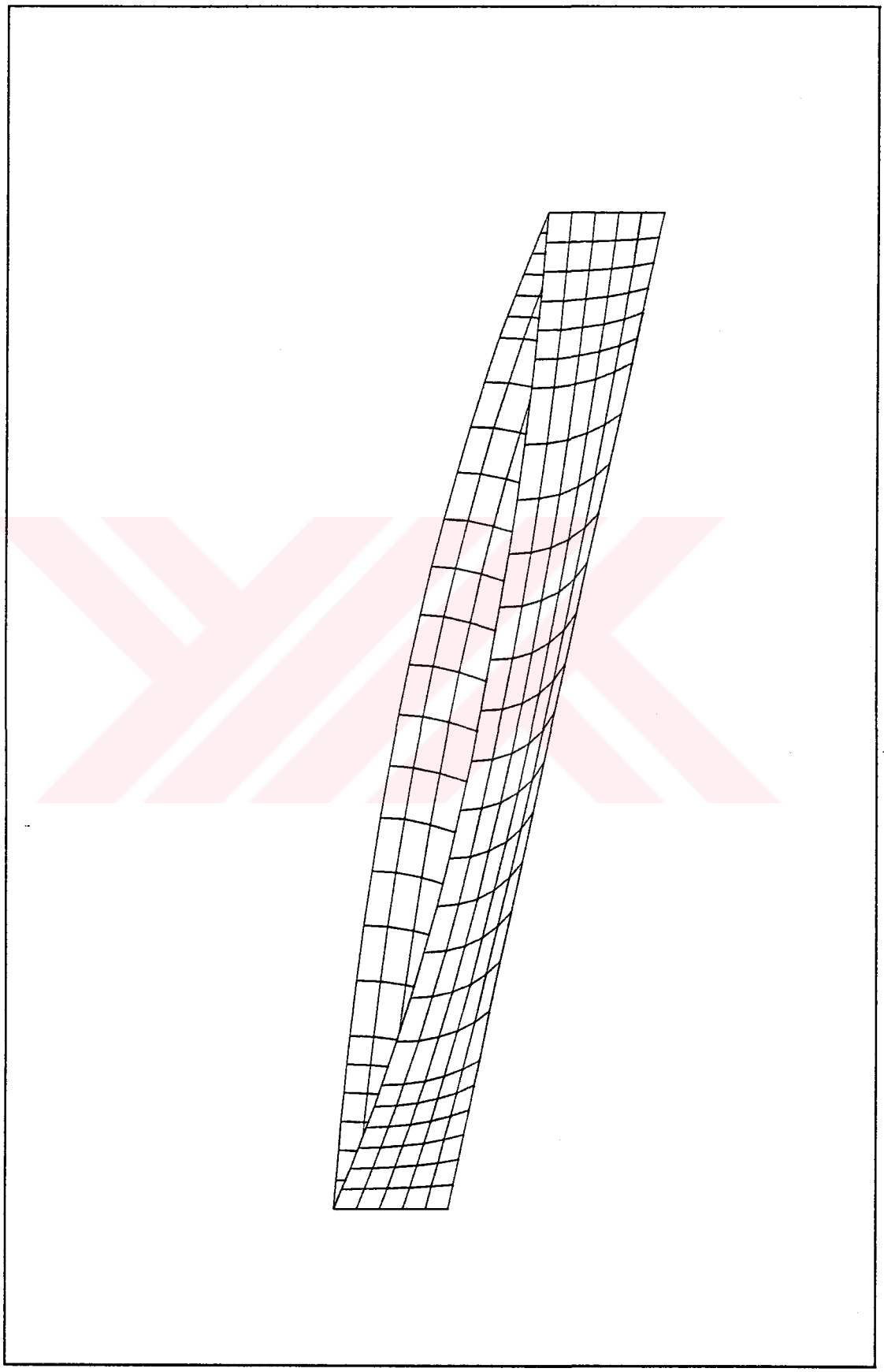

Figure 4-4d. Wigley hull fourth panel arrangement on the ship hull surface.

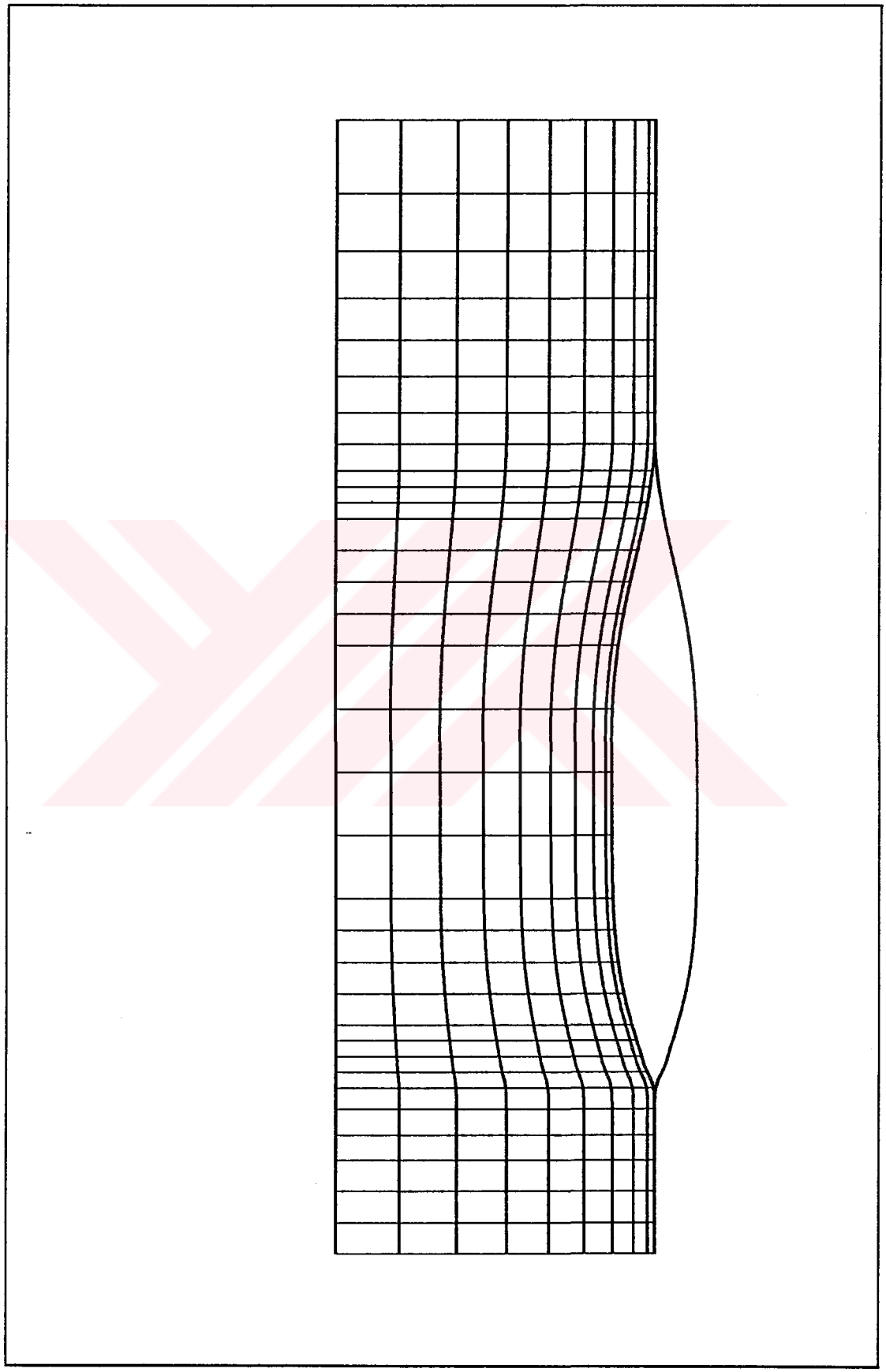

Figure 4-5a. Series-60 hull panel arrangement on the free surface.

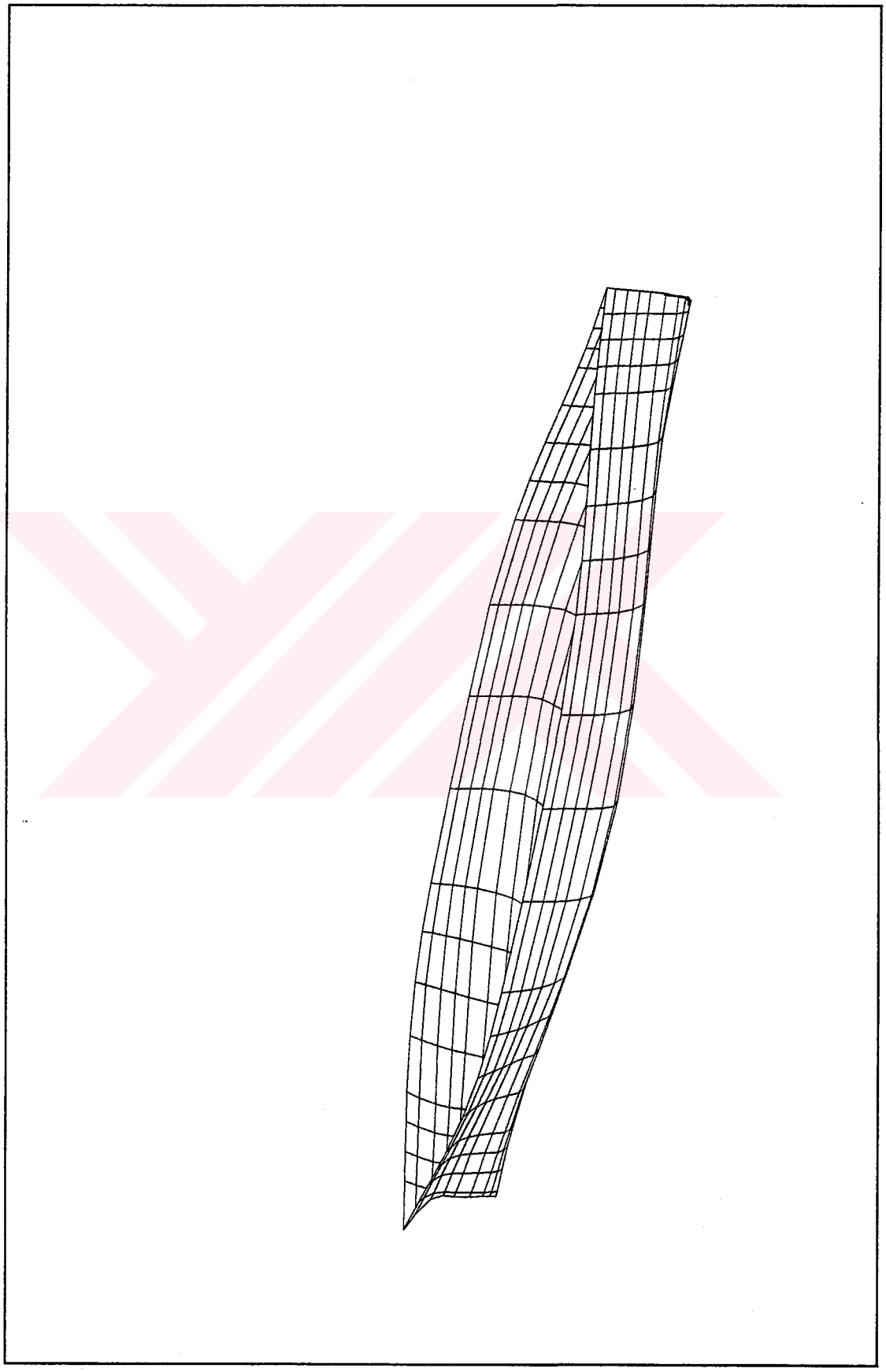

Figure 4-5b. Series-60 hull panel arrangement on the ship hull surface.

4.3. Comparison of Numerical Results with Experimental Data

The present singularity method distributes sources on the ship hull to form a stream surface for the wetted ship surface. The distribution of sources on the ship hull and the velocity potential on the wetted surface are calculated by satisfying the linearized free surface condition and the exact hull boundary condition. From the resulting velocity potential, calculations are made to find the pressure distribution, wave profile, velocity field and sinkage and trim.

There is a large increase in the resistance due to sinkage and trim. **Dawson (1979)** handled the sinkage and trim by first computing the flow with the ship fixed and then determining the vertical hydrodynamic forces from this calculations. The resulting amount of sinkage and trim needed to balance the vertical forces was then used in positioning the ship for a new computation of the flow field.

Within the constraints of the linear theory, the effects of the sinkage and trim of a ship on the flow field are considered to be of higher order. Hence, the numerical results presented in this study are calculated from the velocity potential generated by only the hull surfaces below the design waterline, in the absence of trim and sinkage.

If one can not predict wave resistance for the fixed model condition, a good prediction for most realistic free-to-trim-and-sink condition is unlikely since one has to use the fixed-model condition as the initial condition of an iterative procedure.

The experimental results contain form resistance and present data for a ship free to trim whereas the calculations were made for a fixed ship. In the experimental data there is a large increase in the resistance due to sinkage and trim.

4.3.a. Wigley's Parabolic Hull

For the Wigley's parabolic hull there are several experimental data. However, experimental measurements do not exist for this model fixed at zero trim and sinkage. It is unfortunate not to have the experimental data for a fixed model, because computations were made for the fixed model condition.

The computed wave resistance curves for the four different panel arrangements are shown in **Figure 4-6.**

The first panel arrangement gives too low values. The second panel arrangement, with smaller panels near the bow and stern regions, gives higher values when compared with the first panel arrangement, but these values are still lower than the minimum experimental data. Third panel arrangement, with more panels equally distributed along the ship hull surface, gives higher values than the second panel arrangement, but these values are still out of the envelope of the experimental data. Fourth panel arrangement, with more and smaller panels near bow and stern regions, gives results that compare well with the experimental data. The calculated values of wave resistance are in good agreement with the measured values at moderate values of Froude number, i.e., below $Fn = 0.35$. At higher values of Froude number the calculated values of wave resistance are lower than those obtained experimentally.

The computed wave profiles along Wigley's parabolic hull for $Fn = 0.266$, $Fn = 0.348$ and $Fn = 0.452$ are shown in **Figures 4-7a** through **4-7c.**

It is shown in **Figure 4-7a** that as the number of panels is increased closer wave elevations to experimental data are obtained. In the middle body region especially the region between $2x/L = -0.3$ and $2x/L = 0.2$ the fourth panel arrangement gives almost exact values for the wave elevation. In the bow region, namely the region between $2x/L = -1.0$ and $2x/L = -0.4$ the computed values underpredict the experimental data. In the stern region the computations underpredict the experimental data between $2x/L = 0.2$ and $2x/L = 0.8$ whereas they overpredict the experimental data between $2x/L = 0.8$ and $2x/L = 1.0$.

As it is shown in **Figure 4-7b** for $Fn = 0.348$ the fourth panel arrangement gives considerably closer values to experimental data between $2x/L = -0.8$ and

$2x/L = -0.4$. The computations overpredict the experimental data at the very stern region, namely in the region between $2x/L = 0.8$ and $2x/L = 1.0$. In other regions the computations underpredict the experimental data.

For $Fn = 0.452$ as shown in **Figure 4-7c** the fourth panel arrangement, which seems to be more closer to the experimental data, gives almost exact values in the region between $2x/L = -0.2$ and $2x/L = 0.2$. In the region between $2x/L = -0.4$ and $2x/L = -0.2$ the computations overpredict the experimental data whereas they underpredict the experimental data in all other regions.

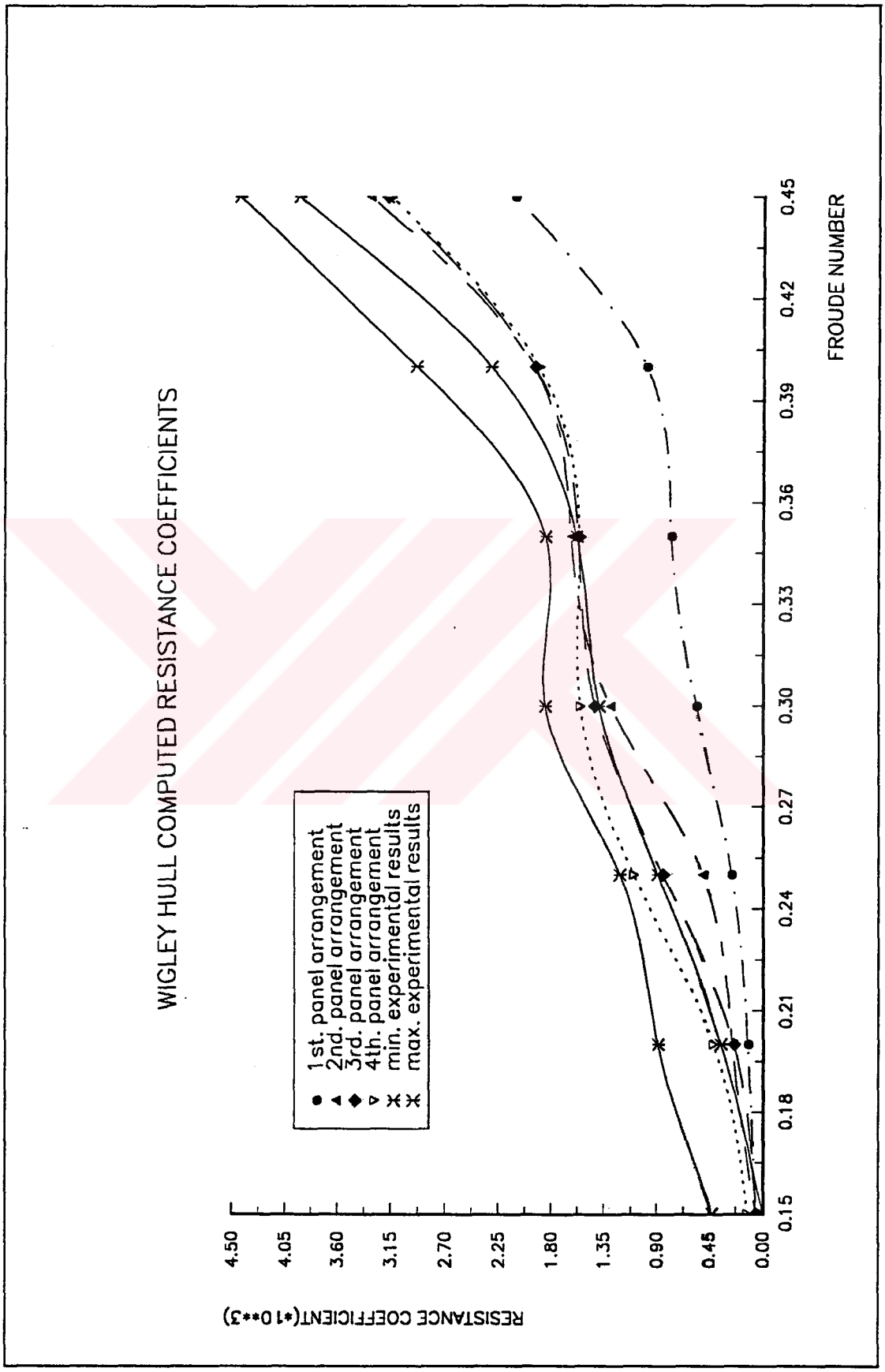

Figure 4-6. Wigley hull computed wave resistance curves.

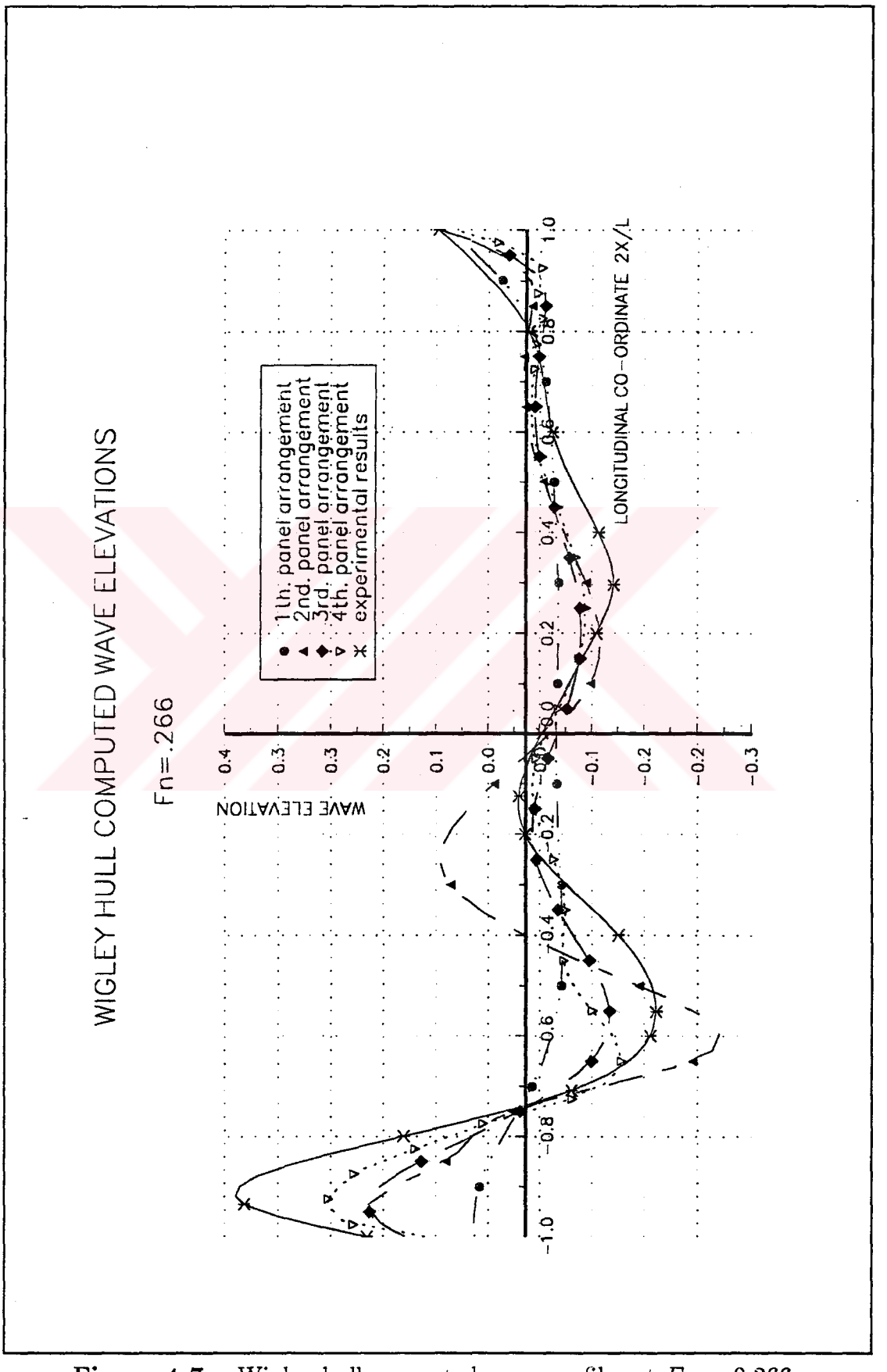

Figure 4-7a. Wigley hull computed wave profiles at $Fn = 0.266$.

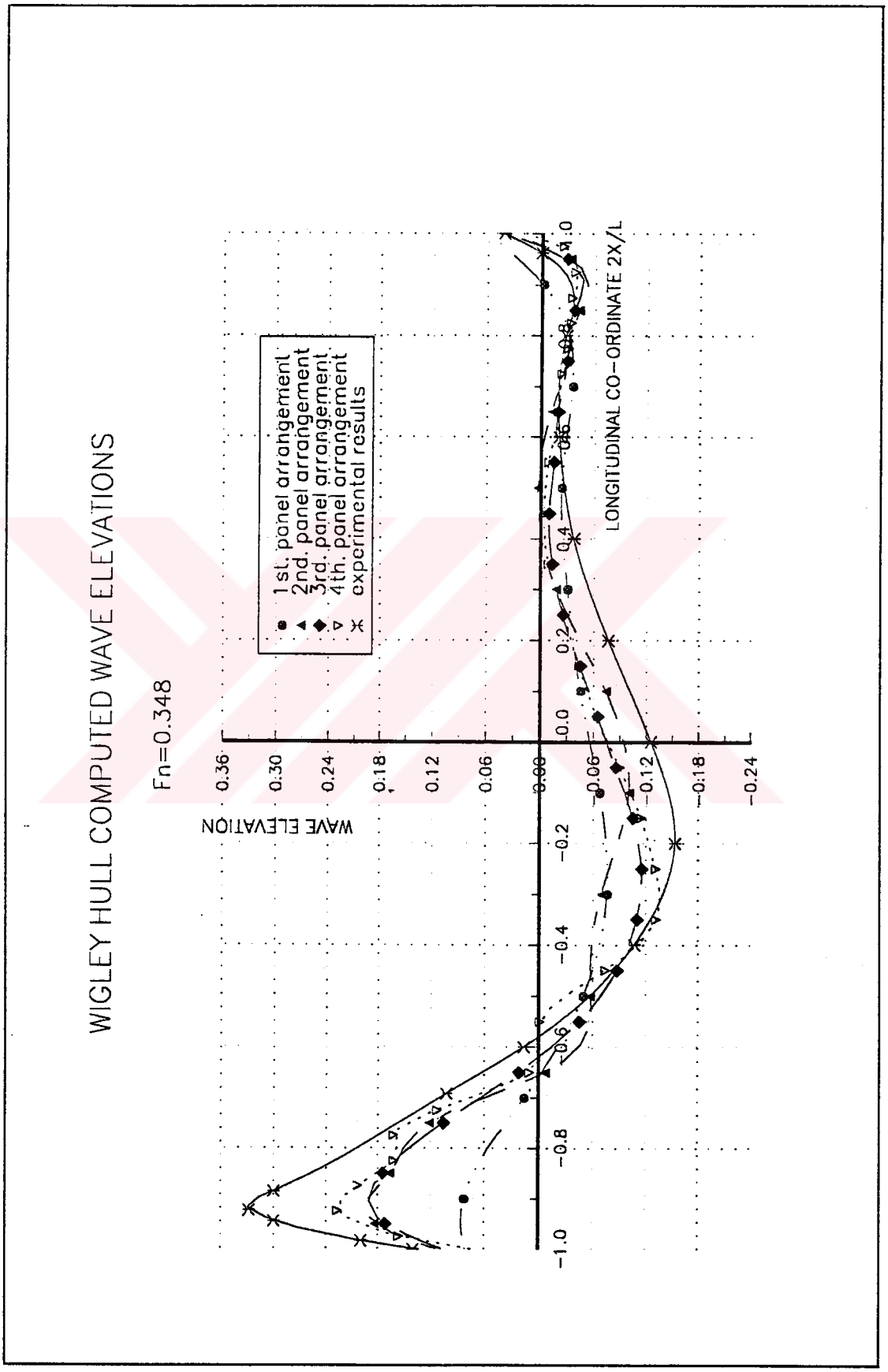

Figure 4-7b. Wigley hull computed wave profiles at $Fn = 0.348$.

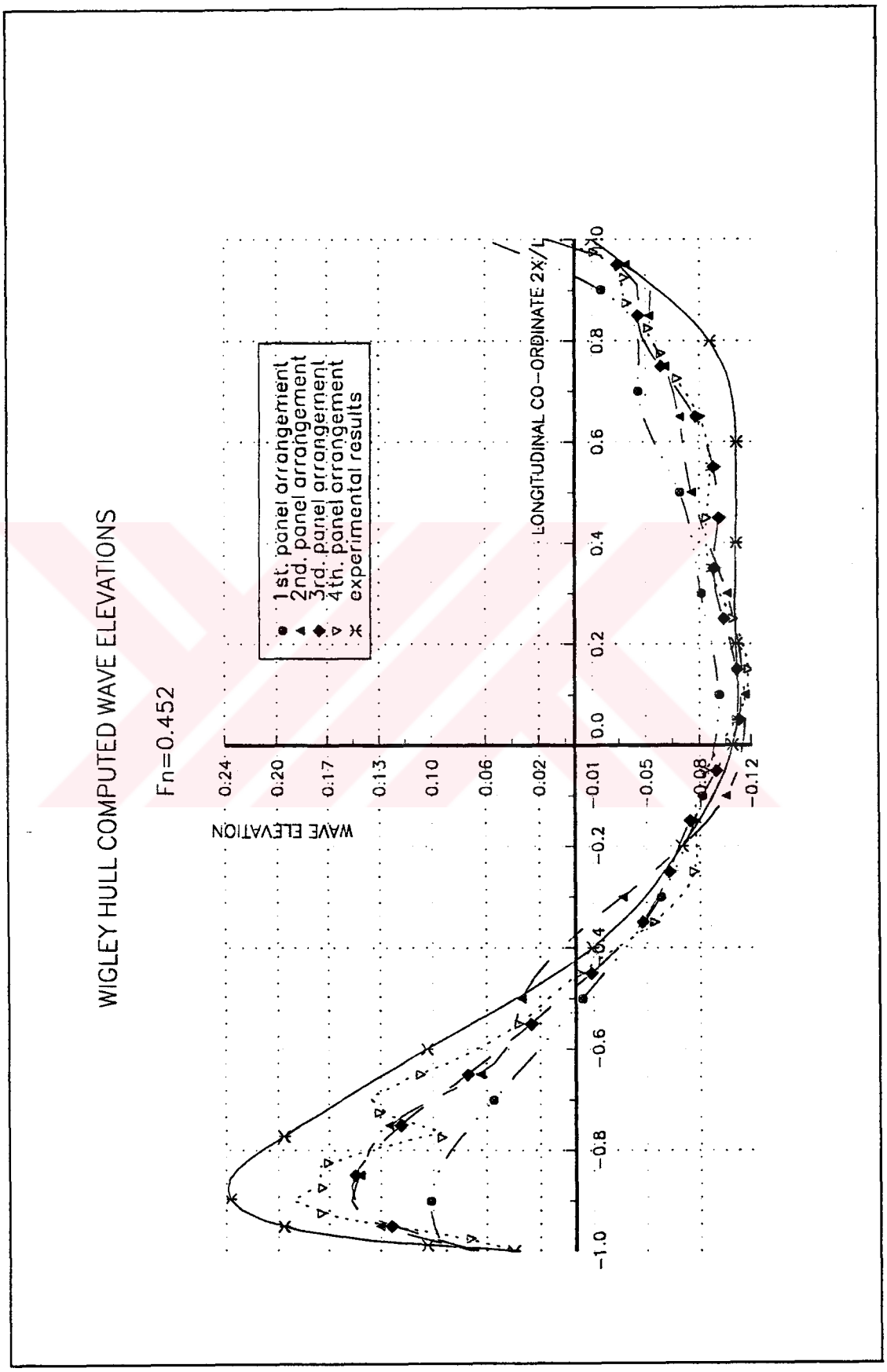

Figure 4-7c. Wigley hull computed wave profiles at $Fn = 0.452$.

4.3.b. Series-60 Hull

For series-60 hull experimental data only for the fixed model is available. Although different panel arrangements are tried, at lower Froude numbers, $Fn \leq 0.2$, negative wave resistance values are obtained as shown in **Figure 4-8**. As the number of panels As the number of panels is increased expected convergence in results is not reached. The wave resistance predictions are not unrealistic though they are underestimated.

For Froude numbers $Fn = 0.22$, $Fn = 0.28$, and $Fn = 0.35$ the computed wave profiles are different from the experimental data as can be seen from **Figures 4-9a** through **4-9c**. These differences are thought to be due to the approach which generates panels on the free surface by using imaginary streamlines.

Then on the free surface, panels are prepared manually by using the real streamlines.† This panel arrangement on the free surface is used together with previously prepared panel distribution on the ship hull surface. By using these data files underestimated but realistic wave profiles are obtained for $Fn = 0.22$, $Fn = 0.28$ and $Fn = 0.35$, respectively. The wave resistance curve is shown in **Figue 4-10**. The wave profiles for $Fn = 0.22$, $Fn = 0.28$ and $Fn = 0.35$ are shown in **Figures 4-11a**, **4-11b** and **4-11c**, respectively.

† graphics obtained from manually prepared data are shown with a (*) at the end.

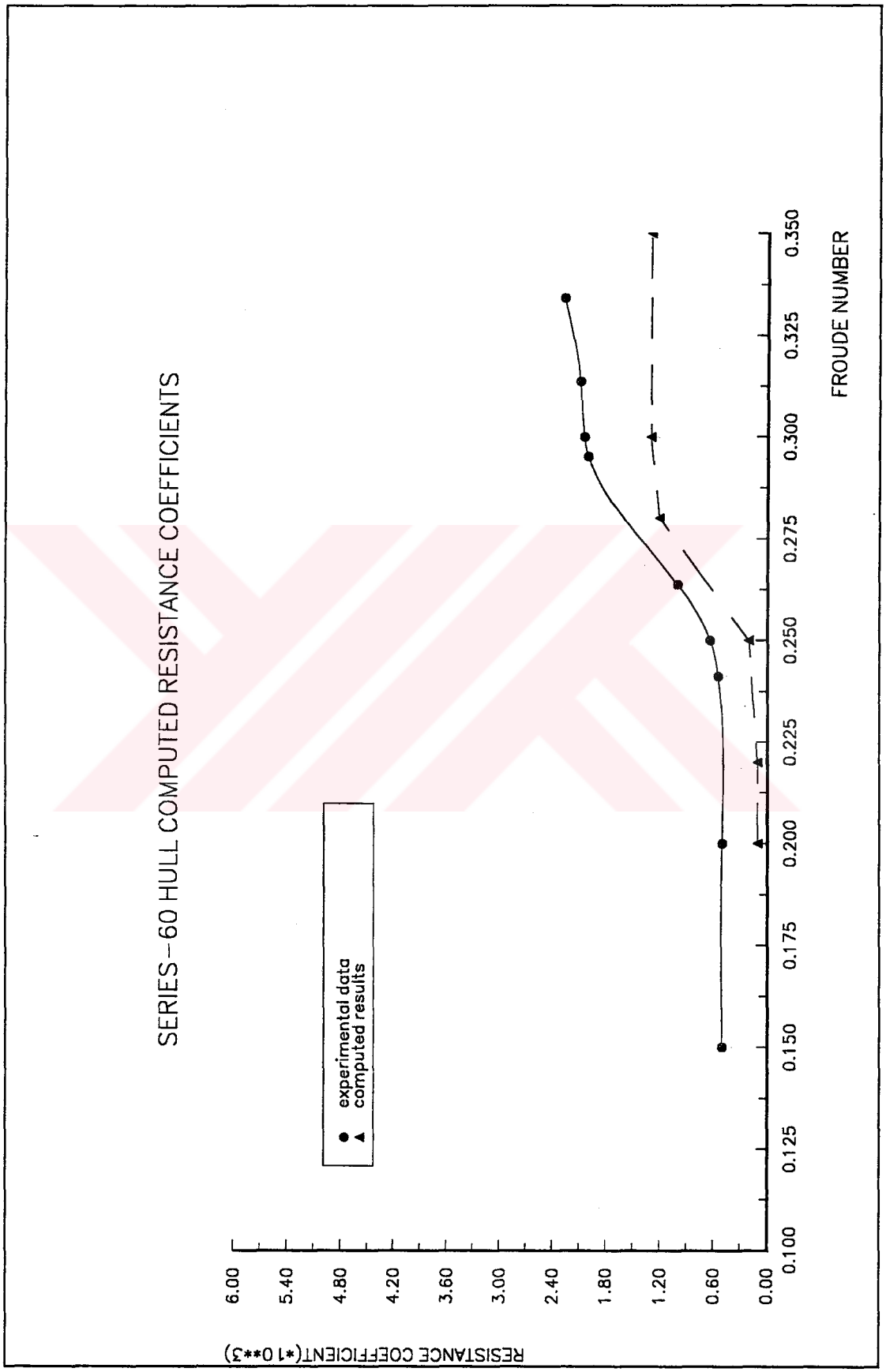

Figure 4-8. Series-60 hull wave resistance curves.

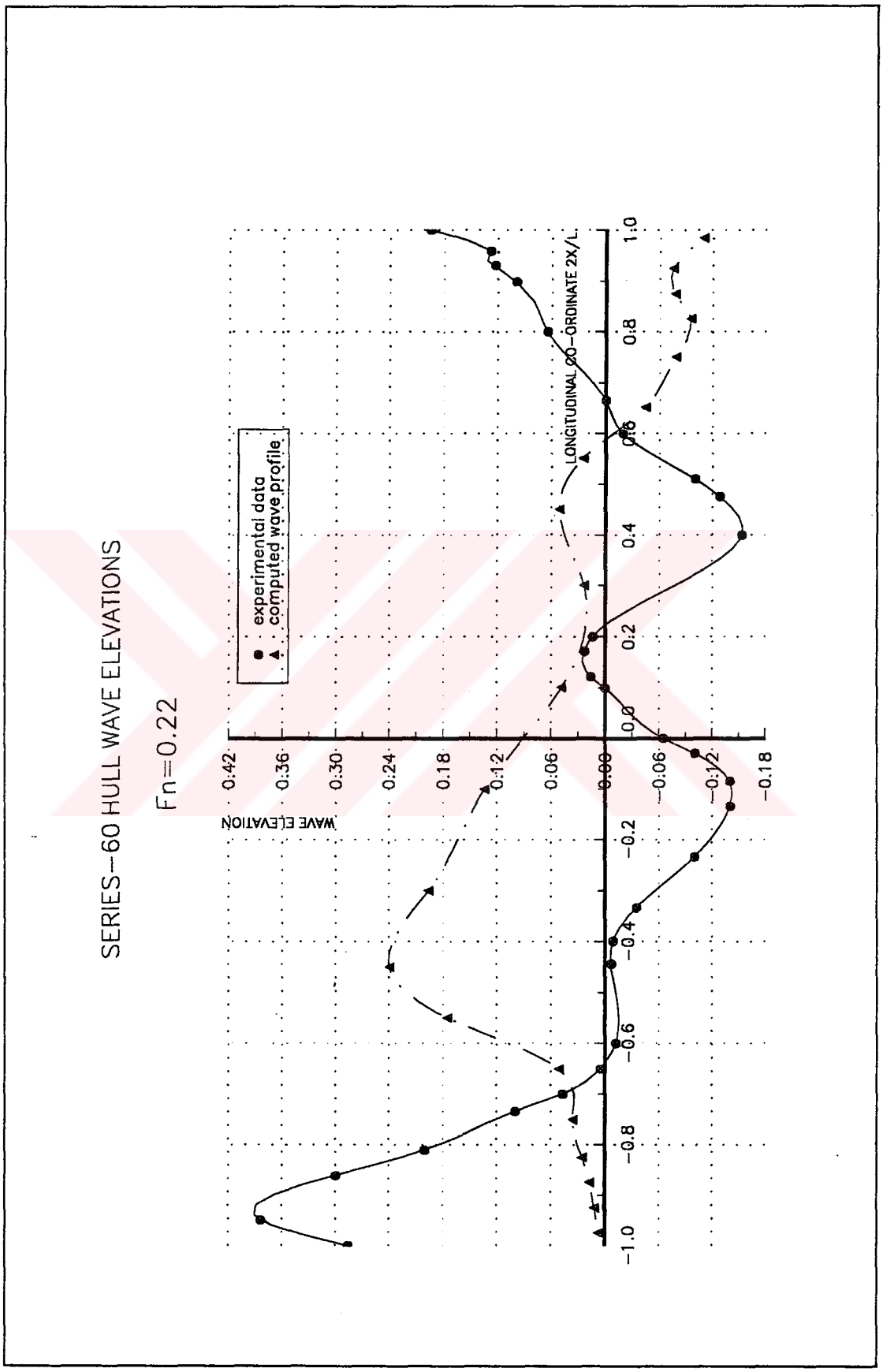

Figure 4-9a. Series-60 hull wave profiles at $Fn = 0.220$.

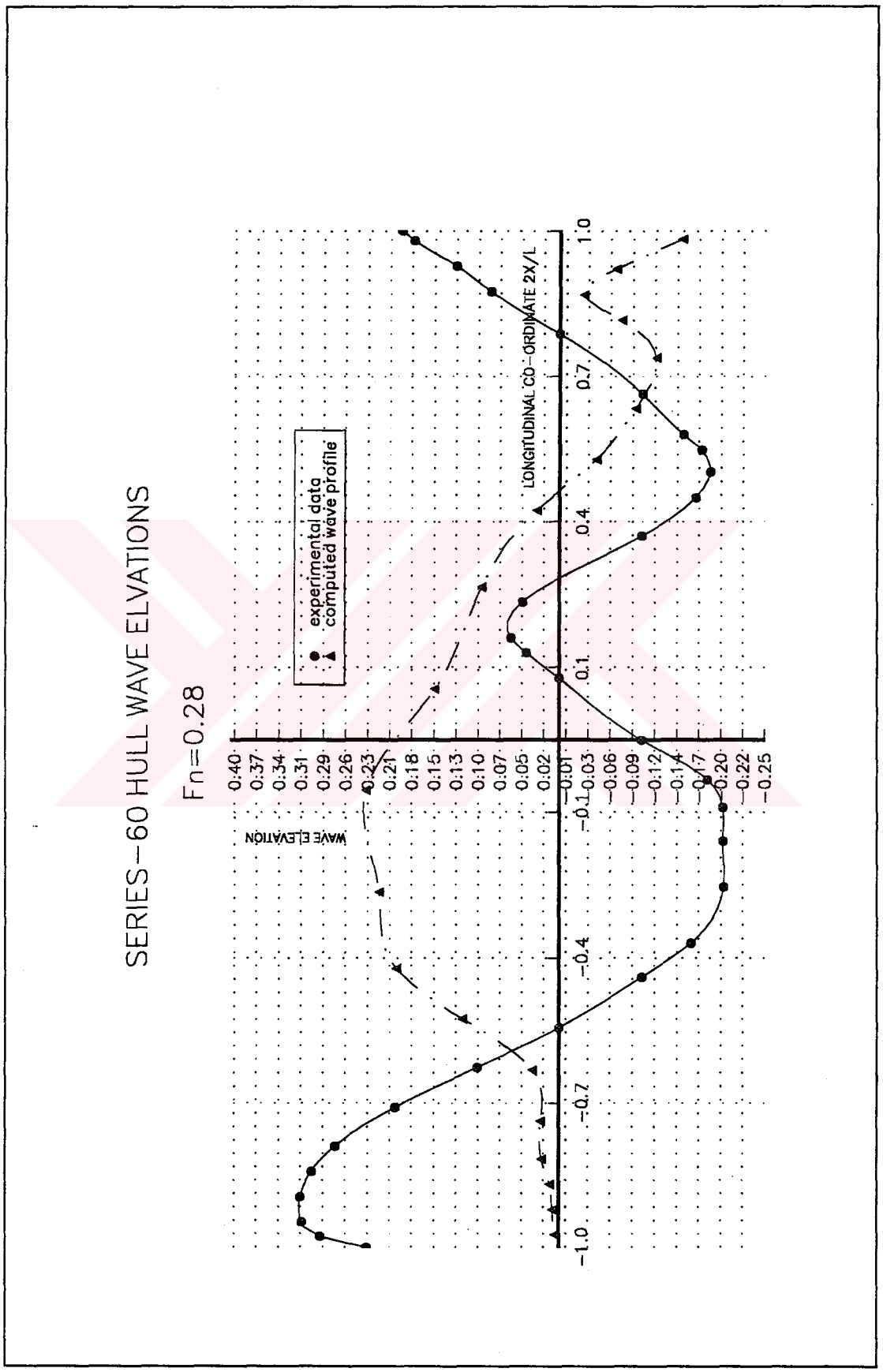

Figure 4-9b. Series-60 hull wave profiles at $Fn = 0.280$.

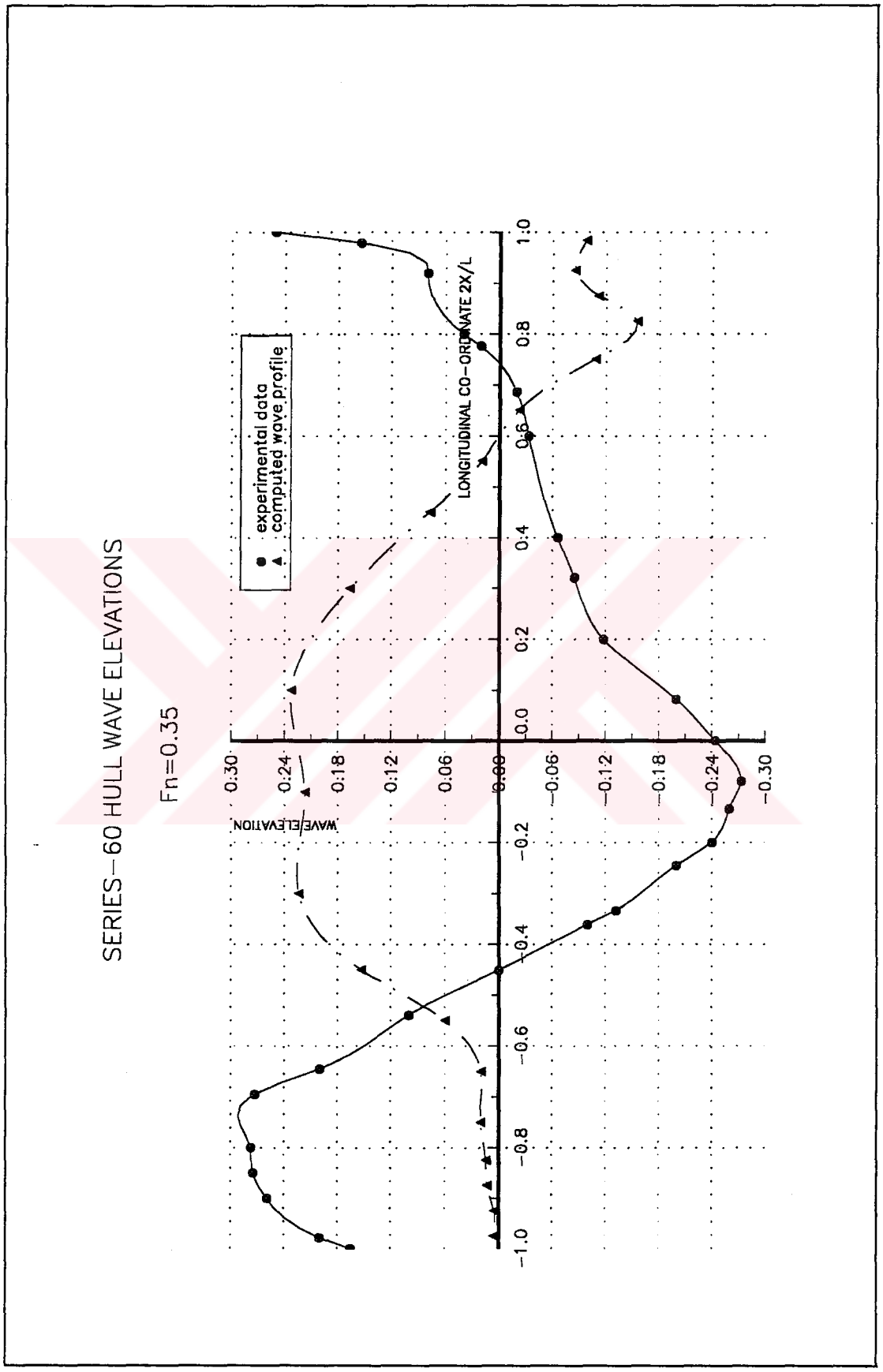

Figure 4-9c. Series-60 hull wave profiles at $Fn = 0.350$.

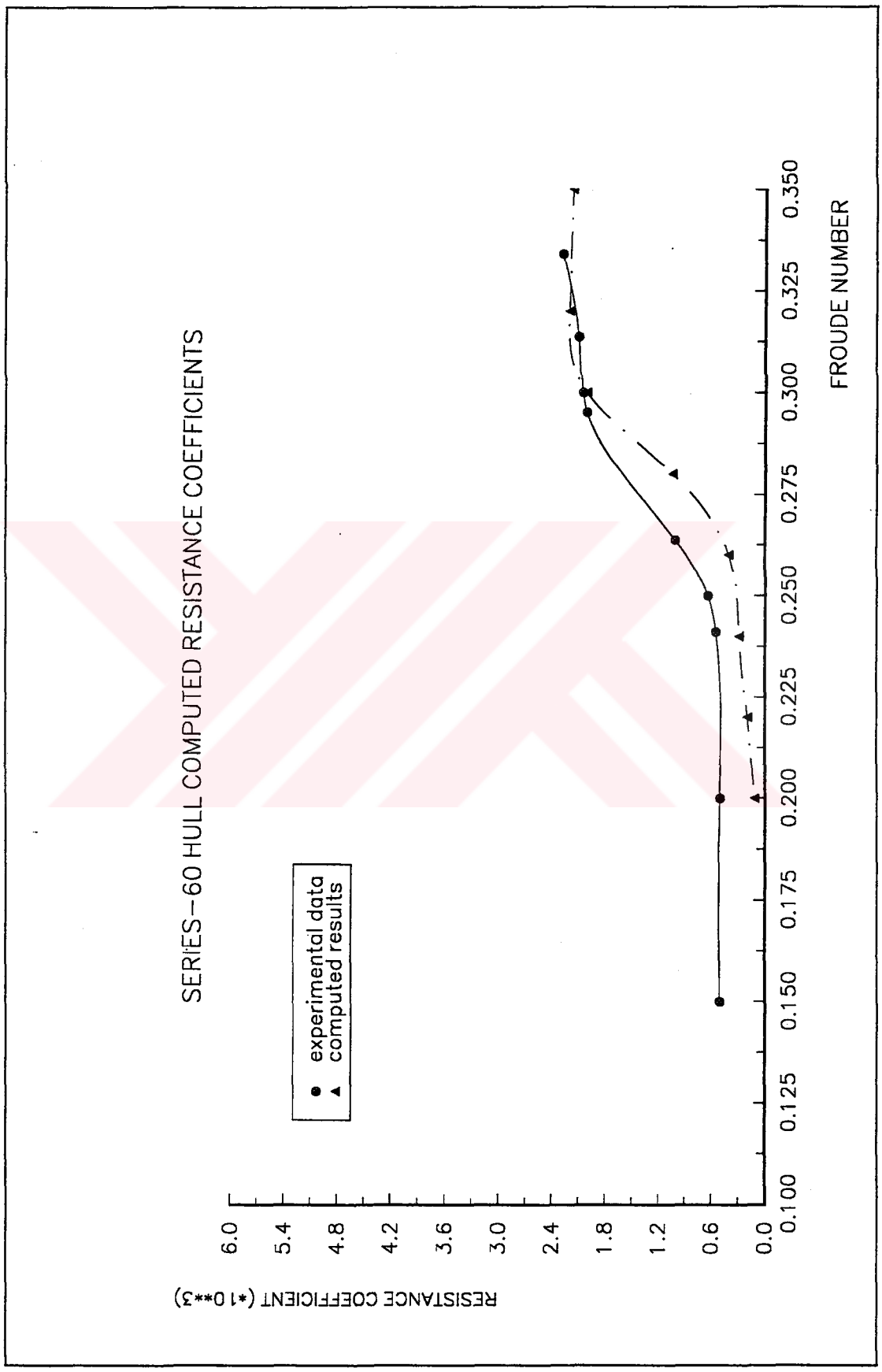

Figure 4-10. Series-60 hull wave resistance curves.*

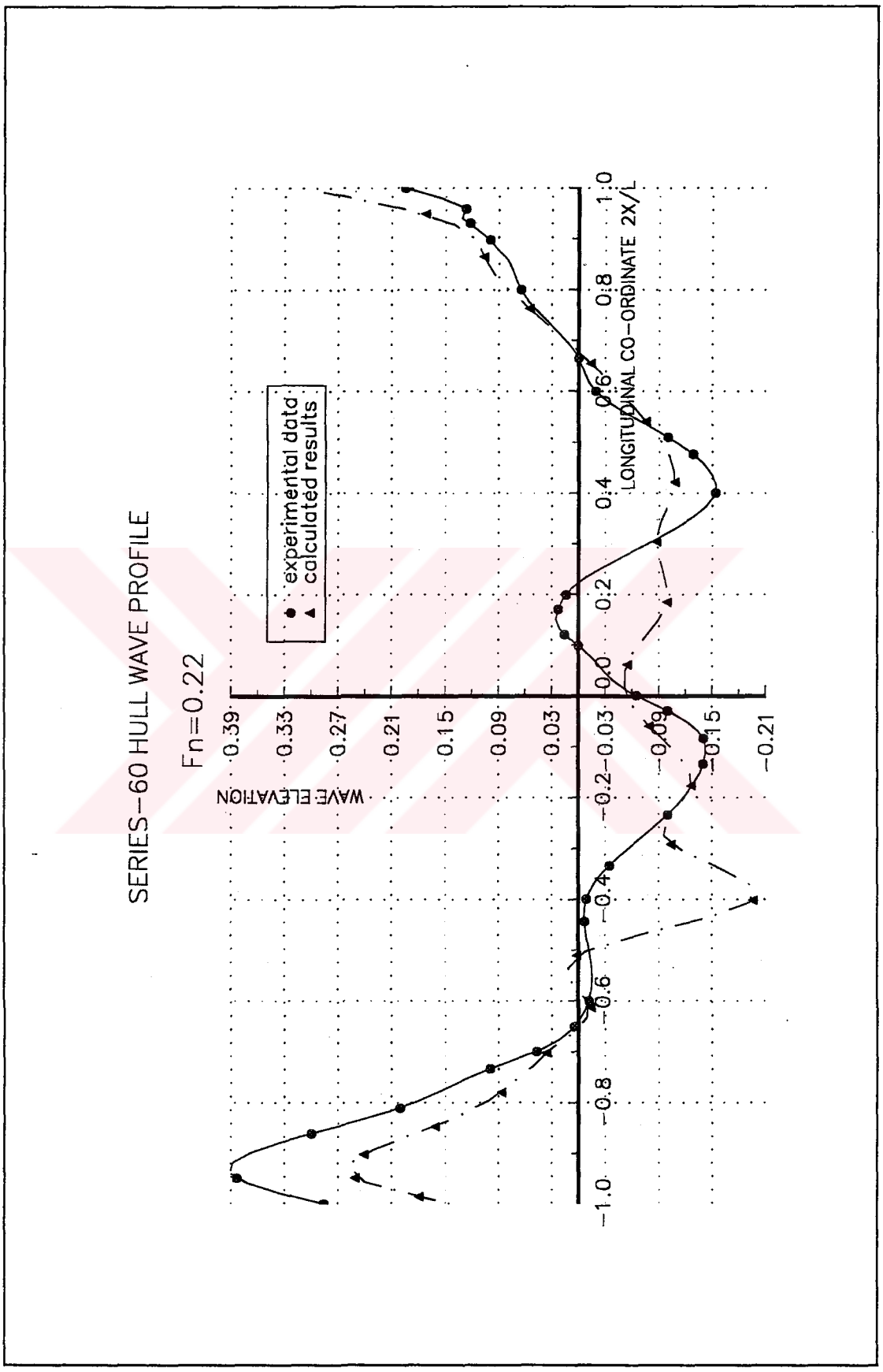

Figure 4-11a. Series-60 hull wave profiles at $Fn = 0.220$.*

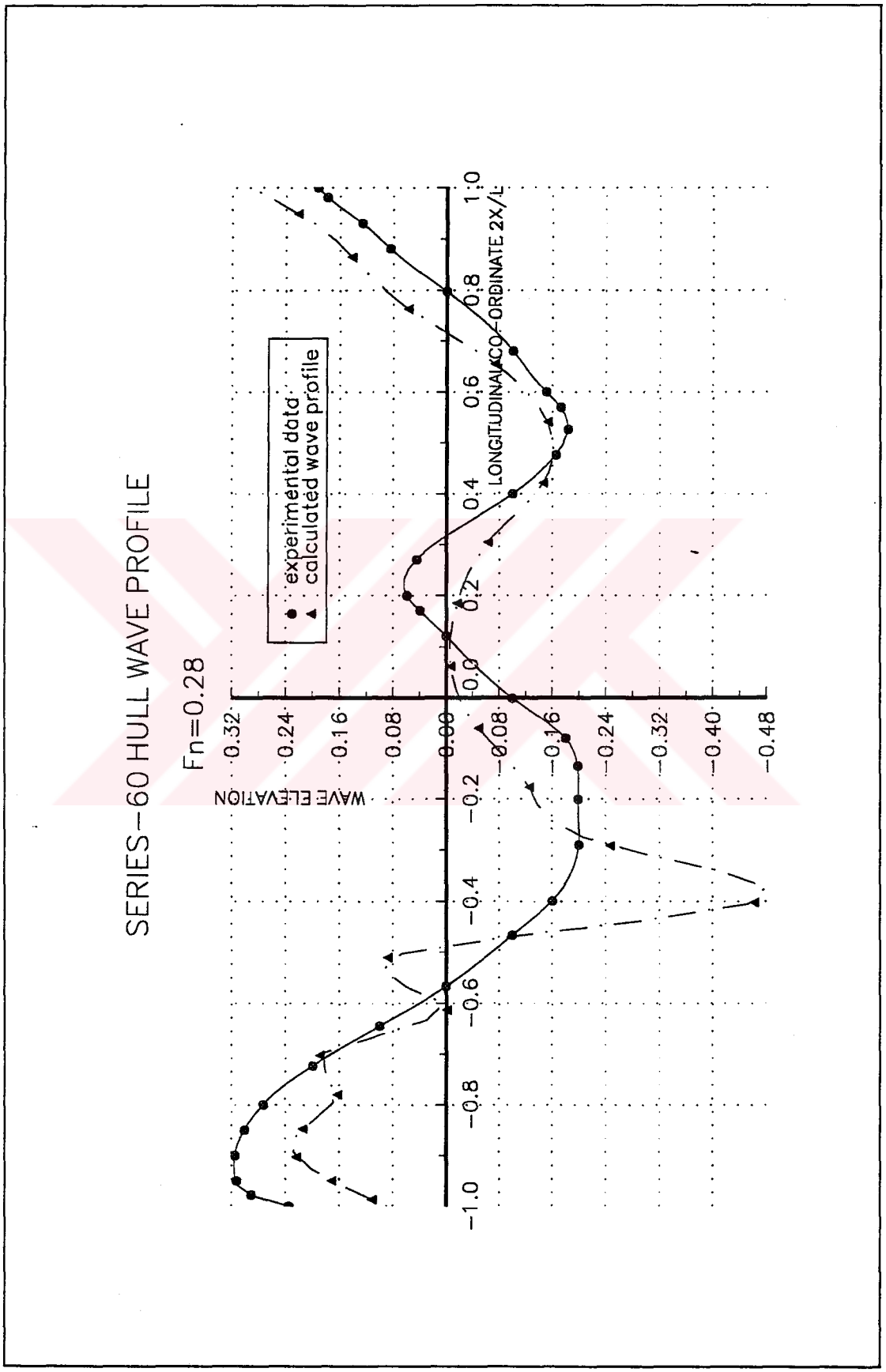

Figure 4-11b. Series-60 hull wave profiles at $Fn = 0.280$.*

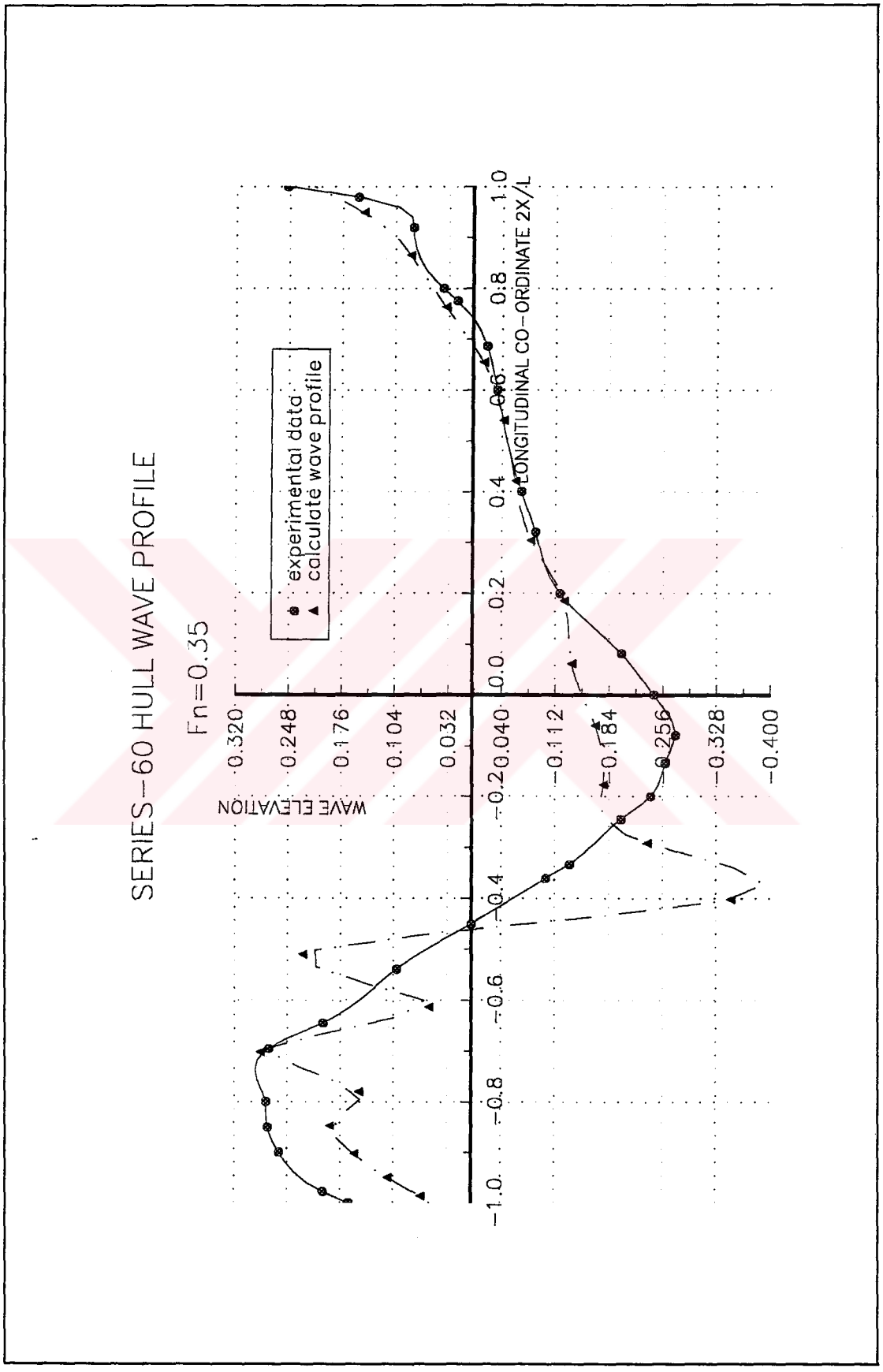

Figure 4-11c. Series-60 hull profiles at $Fn = 0.350$.*

CHAPTER 5. CONCLUDING REMARKS AND RECOMMENDATIONS

With the method of automatic panel generation developed in this study accurate results are obtained for the wave resistance and for the wave profile values. As the number of panels both on the free surface and on the ship hull surface is increased, results that compare well with the experimental data are obtained.

Two preprocessor programmes are developed to prepare input data for the main programme DAWSON.FOR. AutoCAD routines are appended to these programmes to visualize the automatically generated panel arrangement. While developing these programmes, the constraints were the computing time required and the need for visualizing the generated panels. As the number of panels is increased more computing time is required but more accurate results are obtained. On the other hand the need for more panels directed us to use an Apollo HP which has more memory capacity than a PC. But with an Apollo HP it is impossible to use AutoCAD routines and visualize the panels. Hence, we used maximum panels that can be computed by a PC which is a total of 508 panels.

The panels on the ship hull surface are obtained by the intersection of transverse sections and waterlines. For this purpose the transverse sections and the waterlines are defined by spline functions. This intersection gives panels that are almost quadrilateral in shape. But these panels do not represent the hull surface exactly near the regions where the radius of surface curvature suddenly changes, namely near the stern and bow regions.

If the ship hull surface could be paneled by intersecting the transverse sections with waterlines that intersect them orthogonally, the ship hull surface could be defined almost exactly.

With Wigley's parabolic hull results that compare well with the experimental data are obtained. For Series-60 hull unrealistic results are obtained which brings the author to the conclusion that the ship hull surface could not defined exactly by the intersection of transverse sections and waterlines.

Experimental data for the fixed-model condition is needed for both of the models. The effect of sinkage on wave resistance becomes important for the Wigley hull as the Froude number increases. The effect of trim and sinkage is also very important for the Series-60 model.

There is a need for experimental data with Series-60 model fixed to the carriage. Not only residuary resistance curves but also wave resistance coefficients obtained from longitudinal-cut measurements should be given.

Future comparisons of calculation and measurement should be made with a full set of appropriate model observations, including in addition to residuary resistance: wave profiles on and near the hull, trim and wave-probe record. Lacking these, final conclusions regarding the accuracy of calculations will be difficult to make.

Dawson (1979) stated that: "For many problems, the time and labor cost for preparation of the input will be greater than the cost of computer time for running the problems."

The starting point of this work was the above sentence. The aim was to automate this labour. Theoretically, this labour is automated. Four days' time of labour is reduced to 20 minutes of computing time. We believe that this is an important step taken towards filling the gap between numerical calculation schemes and applied research in the field of ship wave-resistance problems.

The achievements and plans for future work are as follows:

i) The aim was to generate panels automatically both on the ship hull surface and on the free surface with a basic input data, which namely is the offsets. This aim is achieved.

ii) This automatization reduced the manual work approximately 80%.

iii) Past computations that were done with manually prepared data showed us that, on the free surface, panels that are generated by using real streamlines gives better resolutions. The approach used in generating the free surface panels

is found to be insufficient for the bluff bodies. Dawson's differentiation scheme, satisfying the free-surface condition, should be used for the solution of the double-model by the panel method.

iv) The preprocessor programmes will be enlarged to generate panels by intersecting transverse sections with waterlines that are orthogonal to them. This will completely terminate the manual work needed in applied research in the ship hull optimization field.

v) A longitudinal cut experiment is done with a Series-60 model at İ.T.Ü. Ata Nutku Towing Tank. After analyzing the obtained data the results will be compared with the computed results obtained by using automatically generated data by the preprocessor programmes. These preprocessor programmes are planned to be used for the verification of the experimental results obtained from the Ata Nutku Towing Tank at İ.T.Ü.

REFERENCES

AMSDEN, A.A., and HIRT, C.W. (1973), *A Simple Scheme for Generating General Curvilinear Grids*, Journal of Computational Physics, Vol. 11, pp. 348-359.

BABA, E., and HARA, M. (1977), *Numerical Evaluation of A Wave-Resistance Theory for Slow Ships*, Proceedings, 2nd. International Conference on Numerical Ship Hydrodynamics, University Extension Pub. Berkeley, Calif., pp. 17-29.

BARFIELD, W.D. (1970), *An Optimal Mesh Generator for Lagrangian Hydrodynamic Calculations in Two-Space Dimensions*, Journal of Computational Physics, Vol. 6, pp. 417-429.

BABUSKA, I., RHEINBOLDT, W., and MESZTENYI, C. (1975), *Self-Adaptive Refinements in the Finite Element Method*, University of Maryland Computer Science, Tech. Rep. TR-375.

CAUGHEY, D.A. (1978), *A Systematic Procedure for Generating Useful Conformed Mappings*, International Journal for Numerical Methods in Engineering, Vol. 12, pp. 1651-1657.

CAVENDISH, J.C. (1974), *Automatic Triangulation of Arbitrary Planar Domains for the Finite Element Method*, International Journal for Numerical Methods in Engineering, Vol. 8, pp. 679-696.

CAVENDISH, J.C. (1975), *Local Mesh Refinement Using Rectangular Blended Finite Elements* , Journal of Computational Physics, Vol. 19, pp.211-228.

CAVENDISH, J.C., GORDON, W.J., and HALL, C.A. (1977), *Substructured Macro Elements Based on Locally Blended Interpolation*, International Journal for Numerical Methods in Engineering, Vol. 11, pp. 1405-1421.

CHENG, B.H. (1989), *Computations of 3D Transom Stern Flows*, Proceedings of the 5th International Conference on Numerical Ship Hydrodynamics, Hiroshima, pp. 522-529.

COOK, W.A. (1974), *Body Oriented (Natural) Co-ordinates for Generating Three-Dimensional Meshes*, International Journal for Numerical Methods in Engineering, Vol. 5, pp. 27-43.

COONS, S.A. (1967), *Surfaces for Computer-Aided Design of Space Forms*, MAC-TR-41.

ÇALIŞAL, S.M., GÖREN, Ö., and OKAN, B. (1991), *On an Iterative Solution for Nonlinear Wave Calculations*, Journal of Ship Research, Vol. 35, No. 1, pp. 9-14.

DAUBE, O. (1980), *Calcul Non Linéaire de la Résistance de Vagues d'un Navire*, Comptes Redus de l'Académie des Sciences, Paris, Vol. 290, pp. 235-238.

DAWSON, C.,W. (1977), *A Practical Computer Method for Solving Ship-Wave Problems*, Proceedings of the 2nd. International Conference on Numerical Ship Hydrodynamics, University of California, Berkeley, pp. 30-38.

DAWSON, C.W. (1979), *Calculation with the XYZ Free Surface Program for Five Ship Models*, Proceedings of the Workshop on Ship Wave-Resistance Computations, David W. Taylor Naval Research and Development Centre, Bethesda, Vol.2, pp. 232-255.

FREY, W.H. (1977), *Flexible Finite-Difference Stencils from Isoparametric Finite Elements*, International Journal for Numerical Methods in Engineering, Vol. 11, pp. 1653-1665.

FRITTS, M.J., and BORIS, J.P. (1979), *The Lagrangian Solution of Transient Problems in Hydrodynamics Using a Triangular Mesh*, Journal of Computational Physics, Vol. 31, pp. 173-215.

GADD, G.E. (1976), *A Method of Computing the Flow and Surface Wave Pattern Around Full Forms*, Transactions of R.I.N.A., Vol.118, pp. 207-219.

GORDON, W.J., and HALL, C.A. (1973), *Construction of Curvilinear Co-ordinate Systems and Applications to Mesh Generation*, International Journal for Numerical Methods in Engineering, Vol. 7, pp. 461-477.

HALL, C.A., LUCZAK, R.W., and SERDY, A.G. (1976), *Numerical Solution of Steady State Heat Flow Problems Over Curved Domains*, ACM Transactions of Mathematical Software, Vol. 2, pp. 257-274.

HAUSSLING, H.J. (1979), *Boundary-Fitted Co-ordinates for Accurate Numerical Solution of Multi-body Flow Problems*, Journal of Computational Physics, Vol. 30, pp.107-124.

HESS, J.L., and SMITH, A.M.O. (1966), *Calculation of Potential Flow About Arbitrary Bodies*, Progress in Aeronautical Science, Vol. 8, pp. 1-138.

KELLOGG, O.D. (1929), *Foundations of Potential Theory*, Frederick Ungar Publishing Co., Chapter 11, New York. [Also available from Dover Publications, Inc., New York.]

LAU, P.C.M. (1979), *Curvilinear Finite Difference Method for Three-Dimensional Potential Problems*, Journal of Computational Physics, Vol. 32, pp. 325-344.

LINDENMUTH, W.T., RATCLIFFE, T.J., and REED, A.M. (1991), *Comparative Accuracy of Numerical Kelvin Wake Code Predictions-Wake off*, David Taylor Research Centre Report, DTRC 91/004, Bethesda, Md.

McNEICE, G.M., and MARCAL, P.V. (1971), *Optimization of Finite Element Grids Based on Minimum Potential Energy*, Tech. Rep. No. 7, Division of Engineering, Brown University, Department of the Navy, Office of Naval Research.

NAKATAKE, K., ANDO, J., KATAOKA, K., and ODA, K. (1991), *Numerical Calculation of Free Surface Effect on Propulsive Performance of Ships*, Memoirs of the Faculty of Engineering, Kyushu University, Vol. 51, No. 4, pp. 330-354.

PAVLIN, V., and PERRONE, N. (1979), *Finite-Difference Energy Techniques for Arbitrary Meshes Applied to Linear Plate Problems*, International Journal for Numerical Methods in Engineering, Vol. 14, pp. 647-664.

POPE, S.B. (1978), *The Calculation of Turbulent Recirculating Flows in General Orthogonal Co-ordinates*, Journal of Computational Physics, Vol. 26, pp.197-217.

YANENKO, N.N., KROSHKO, E.A., LISEIKIN, V.V., FOMIN, V.M., SHAPEEV, V.P., and SHITOV, Y.A. (1976), *Methods fot the Construction of Moving Grids for Problems of Fluid Dynamics with Big Deformations*, Proceedings of the 5th. International Conference on Numerical Methods in Fluid Dynamics, Twente University, Enschede.

ZIENKIEWICZ, O.C. (1971), *The Finite Element Method in Engineering Science*, McGraw-Hill, New York.

ZIENKIEWICZ, O.C., and PHILLIPS, D.V. (1971), *An Automatic Mesh Generation Scheme for Plane and Curved Surfaces by 'Isoparametric' Coordinates*, International Journal for Numerical Methods in Engineering, Vol. 3, pp. 519-528.

APPENDIX A

WIGLEY's PARABOLIC HULL

Hull Geometry

$$B/L = 0.1000$$

$$H/L = 0.0625$$

$$C_B = 0.4440$$

$$C_{PR} = 0.6670$$

$$C_X = 0.6670$$

$$C_S = 0.6610$$

$$L/L_{PP} = 1.0000$$

NOTE: The hull surface is shown in **Figure A.1** and is defined by:

$$y = \frac{B}{2}\{1 - (\frac{2x}{L})^2\}\{1 - (\frac{z}{H})^2\}$$

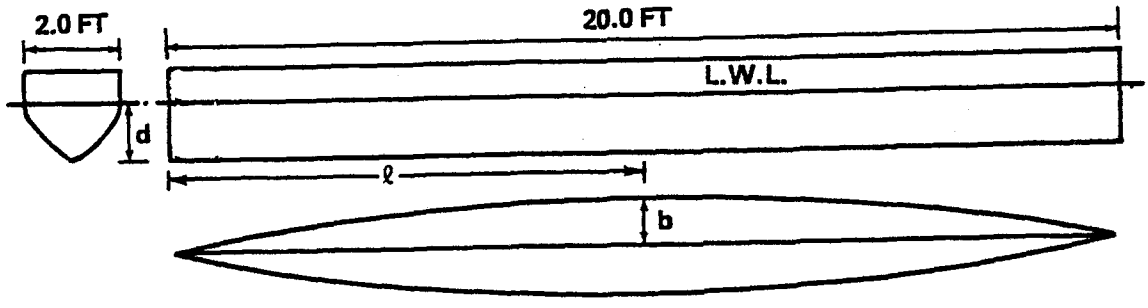

Figure A.1. Wigley hull form.

APPENDIX B

SERIES 60, $C_B = 0.60$ (PARENT FORM-MODEL 4210W)

Hull Geometry

$$B/L_{PP} = 0.1333$$

$$H/L_{PP} = 0.0533$$

$$C_B = 0.6000$$

$$C_{PR} = 0.6140$$

$$C_X = 0.9770$$

$$C_S = 0.7100$$

$$L/L_{PP} = 1.0167$$

NOTE: L_{PP} is used in defining all of the hull characteristics. **Table B-1** gives offsets.

Table B-1. Series-60 hull offsets.

Sta	*Tan.*	0.075	0.250	0.500	0.750	1.000	1.250	1.500	A/A_{WL}
FP	0.000	0.000	0.000	0.000	0.000	0.000	0.020	0.042	0.000
0.5	0.009	0.032	0.042	0.041	0.043	0.051	0.076	0.120	0.042
1	0.013	0.064	0.082	0.087	0.090	0.102	0.133	0.198	0.085
1.5	0.019	0.095	0.126	0.141	0.148	0.160	0.195	0.278	0.135
2	0.024	0.127	0.178	0.204	0.213	0.228	0.270	0.360	0.192
3	0.055	0.196	0.294	0.346	0.368	0.391	0.440	0.531	0.323
4	0.134	0.314	0.436	0.502	0.535	0.562	0.607	0.683	0.475
5	0.275	0.466	0.589	0.660	0.691	0.718	0.754	0.804	0.630
6	0.469	0.630	0.733	0.802	0.824	0.841	0.862	0.889	0.771
7	0.666	0.779	0.854	0.906	0.917	0.926	0.936	0.946	0.880
8	0.831	0.898	0.935	0.971	0.977	0.979	0.981	0.982	0.955
9	0.945	0.964	0.979	0.996	1.000	1.000	1.000	1.000	0.990
10	1.000	1.000	1.000	1.000	1.000	1.000	1.000	1.000	1.000
11	0.965	0.982	0.990	1.000	1.000	1.000	1.000	1.000	0.996
12	0.882	0.922	0.958	0.994	1.000	1.000	1.000	1.000	0.977
13	0.767	0.826	0.892	0.962	0.987	0.994	0.997	1.000	0.938
14	0.622	0.701	0.781	0.884	0.943	0.975	0.990	0.999	0.863
15	0.463	0.560	0.639	0.754	0.857	0.937	0.977	0.994	0.750
16	0.309	0.413	0.483	0.592	0.728	0.857	0.933	0.975	0.609
17	0.168	0.267	0.330	0.413	0.541	0.725	0.844	0.924	0.445
18	0.065	0.152	0.193	0.236	0.321	0.536	0.709	0.834	0.268
18.5	0.032	0.102	0.130	0.156	0.216	0.425	0.626	0.769	0.187
19	0.014	0.058	0.076	0.085	0.116	0.308	0.530	0.686	0.109
19.5	0.010	0.020	0.020	0.022	0.033	0.193	0.418	0.579	0.040
AP	0.000	0.000	0.000	0.000	0.000	0.082	0.270	0.420	0.004
B_{max}	0.710	0.866	0.985	1.000	1.000	1.000	1.000	1.000	

RESUME

Şafak Nur ERTÜRK was born in 1971 in İstanbul. In 1982 she started Beyoğlu Anadolu Lisesi and graduated in 1989. At the same year she passed the university entrance examinations and started to study at İstanbul Technical University. In June 1993 she graduated as a Naval Architect and Ocean Engineer. She took a schoolar-ship from the Turkish Petroleum Foundation during her secondary and university education periods. In October 1993 she began to make her M.Sc. degree in İstanbul Technical University Institute of Science and Technology. In January 1994 she started to work as a Research Assistant at the Ocean Engineering Department of İstanbul Technical University Faculty of Naval Architecture and Ocean Engineering.